

Stable approximation of Helmholtz solutions by evanescent plane waves

Emile Parolin¹, Daan Huybrechs², and Andrea Moiola³

¹Università di Pavia, Pavia, Italy, emile.parolin@unipv.it

²KU Leuven, Leuven, Belgium, daan.huybrechs@kuleuven.be

³Università di Pavia, Pavia, Italy, andrea.moiola@unipv.it

February 14, 2022

Abstract

Solutions of the Helmholtz equation are known to be well approximated by superpositions of propagative plane waves. This observation is the foundation of successful Trefftz methods. However, when too many plane waves are used, the computation of the expansion is known to be numerically unstable. We explain how this effect is due to the presence of exponentially large coefficients in the expansion and can drastically limit the efficiency of the approach.

In this work, we show that the Helmholtz solutions on a disk can be exactly represented by a continuous superposition of evanescent plane waves, generalizing the standard Herglotz representation. Here, by evanescent plane waves, we mean exponential plane waves with complex-valued propagation vector, whose absolute value decays exponentially in one direction. In addition, the density in this representation is proved to be uniformly bounded in a suitable weighted Lebesgue norm, hence overcoming the instability observed with propagative plane waves and paving the way for stable discrete expansions.

In view of practical implementations, discretization strategies are investigated. We construct suitable finite-dimensional sets of evanescent plane waves using sampling strategies in a parametric domain. Provided one uses sufficient oversampling and regularization, the resulting approximations are shown to be both controllably accurate and numerically stable, as supported by numerical evidence.

Keywords: Helmholtz equation, Plane waves, Evanescent waves, Trefftz method, Stable approximation, Sampling, Frames, Reproducing kernel Hilbert spaces, Herglotz representation

AMS subject classification: 35J05, 41A30, 42C15, 44A15

Contents

1	Introduction	3
1.1	Approximation of Helmholtz solutions	3
1.2	Plane wave instability and the quest for stable approximation	3
1.3	Stable approximations from ill-conditioned linear systems	4
1.4	Main results	5
1.5	Outline of the paper	6
2	Helmholtz equation in circular geometry	7
2.1	Circular waves	7
2.2	Asymptotics of normalization coefficients	9
3	Stable numerical approximation	10
3.1	The notion of stable approximation	10
3.2	Boundary sampling method	11
3.3	Regularization	12
3.4	Error estimates for the sampling method with regularization	13
4	Instability of propagative plane wave sets	15
4.1	Propagative plane waves	15
4.2	Herglotz representation	16
4.3	Propagative plane waves do not give stable approximations	17
4.4	Numerical illustration	19
5	Evanescent plane waves	21
5.1	Definition	21
5.2	Modal analysis of evanescent plane waves	21
6	Mapping Herglotz densities to Helmholtz solutions	22
6.1	Space of Herglotz densities	23
6.2	Herglotz transform	25
6.3	The reproducing kernel property	28
7	A concrete evanescent plane wave approximation set	29
7.1	Truncation of the modal expansion	29
7.2	Parameter sampling in the cylinder Y	30
7.3	Stability of evanescent plane wave sets	32
8	Numerical results	33
8.1	Probability densities and samples	33
8.2	Evanescent plane waves are stable	36
8.3	Approximation of solution surrogates	39
8.4	Numerical evidence of quasi-optimality	41
9	Conclusions	43
	References	43

1 Introduction

1.1 Approximation of Helmholtz solutions

The homogeneous Helmholtz equation

$$-\Delta u - \kappa^2 u = 0 \quad (1.1)$$

is a fundamental equation in computational acoustics. It characterizes the space dependence of time-harmonic solutions $U(\mathbf{x}, t) = \Re\{e^{-i\omega t}u(\mathbf{x})\}$ of the scalar wave equation $\frac{1}{c^2}\frac{\partial^2 U}{\partial t^2} - \Delta U = 0$. The wavenumber is $\kappa = \omega/c > 0$, where c is the wave speed and ω the time frequency. The numerical approximation of solutions of boundary value problems for the Helmholtz equation is notoriously difficult and computationally expensive at high frequencies, namely when the wavelength $\lambda = 2\pi/\kappa$ is much smaller than the characteristic length of the computational domain. A major difficulty is related to approximation: Helmholtz solutions are highly oscillatory and their approximation with (piecewise) polynomials requires large numbers of degrees of freedom.

A well-studied way to represent Helmholtz solutions in a domain of \mathbb{R}^n is to approximate them with linear combinations of propagative plane waves $\mathbf{x} \mapsto e^{i\kappa \mathbf{d} \cdot \mathbf{x}}$, for different propagation directions $\mathbf{d} \in \mathbb{R}^n$ with $\mathbf{d} \cdot \mathbf{d} = 1$. The main reason is that plane waves offer better accuracy for fewer degrees of freedom in comparison to polynomial spaces: the theory developed in [27], building on previous results of [26, Sec. 8.4] and [6, Sec. 3.3.5], guarantees that any Helmholtz solution with a certain Sobolev regularity can be efficiently approximated by plane waves.

Approximation by plane waves has been extensively used in the context of Trefftz methods. These are discretization schemes that use trial and test functions that are piecewise (on each element of a mesh) solution of the PDE to be approximated, in this case the Helmholtz equation. Many Trefftz methods for the Helmholtz equation have been developed, see [20] for a survey and more than a hundred references. A second widespread use of approximation by plane waves is the reconstruction of sound fields from point measurements (representing microphones) in experimental acoustics, possibly without knowing the shape of the domain, see [8, 23, 30, 18].

1.2 Plane wave instability and the quest for stable approximation

When too many plane waves are used, the computation of the expansion is known to be numerically unstable, which can drastically limit the accuracy and the efficiency of plane wave approximations [29, 4]. This issue is often understood as an effect of the ill-conditioning of the linear system that is solved to compute the approximation. Indeed, ill-conditioning necessarily arises from the almost-linear dependence of propagative plane waves with similar directions of propagation, a situation which is unavoidable when increasing the size of the approximation space. Ill-conditioning and instability have been recognized in all plane-wave based Trefftz schemes [20, Sec. 4.3] and are perhaps the main reason that prevented a widespread use of such methods. Different techniques have been proposed to curb this instability, see [3, 12, 4]. A well-known remedy requires using not more than a prescribed number of plane waves in elements of a given size, e.g. [21, eq. (14)]: this keeps the instability at bay but limits the achievable accuracy.

In the context of the “Wave Based Method” (WBM, a special class of Trefftz schemes, see e.g. [14] for a survey) good numerical results are obtained by enriching a propagative plane wave basis with a number of evanescent plane waves. Here, by “evanescent plane wave”, we mean a plane wave whose direction is a complex-valued vector $\mathbf{d} \in \mathbb{C}^n$. The Helmholtz equation is still satisfied provided $\mathbf{d} \cdot \mathbf{d} = 1$. The simple exponential expression allows to implementing Trefftz schemes very cheaply; in particular, the integrals of products of these functions and their derivatives can be computed in closed form and with wavenumber-independent effort, see [20, Sec. 4.1]. Since

their modulus decays exponentially in the direction $\Im[\mathbf{d}]$, evanescent plane waves are localized both in the physical and in the Fourier domain. Therefore, they are natural candidates for the approximation of the high-frequency angular content exhibited by certain Helmholtz solutions. The main difficulty is to select suitable values for \mathbf{d} , while maintaining a moderate size for the approximation space. A heuristic, and numerically effective, choice for a set of complex directions \mathbf{d} is suggested in [14, Sec. 3.2] (see also [20, Sec. 3.2]), but no mathematical justification is provided. Evanescent plane waves proved particularly effective in the approximation of interface problems in Trefftz schemes, e.g. [25], and the approximation of integral kernels in some versions of the Fast Multipole Method [7].

Recent advances in the more general setting of approximation theory, in particular using frames, have shown that ill-conditioning can be successfully overcome with regularization techniques, provided there exist accurate approximations in the form of expansions with bounded coefficients [1, 2]. It turns out that, when using propagative plane waves, for some smooth target Helmholtz solutions such approximations do not exist and (exponentially) large coefficients are necessarily present in the expansion. We prove this in the case of a circular domain: the instability is due to the fact that propagative plane waves are inadequate to approximate the evanescent circular modes, i.e. solutions with dominant contributions from large-order Fourier modes.

The main objective of the present paper is to provide a theoretical foundation for the use of evanescent plane waves in the approximation of Helmholtz solutions. We aim to construct approximation sets that allow approximations which are both controllably accurate and stable, in the sense of allowing expansions with bounded coefficients for Helmholtz solutions with bounded norms. This concept of stability is useful when computing approximations numerically, because the boundedness of the coefficients allows to preserving accuracy also in finite-precision arithmetic, regardless of the condition number of the linear system involved.

As a first step in this direction, we focus on the model approximation problem of Helmholtz solutions in the unit disk. Approximation properties of solutions in more general domains will be considered in the future.

1.3 Stable approximations from ill-conditioned linear systems

We briefly remark on how the above-mentioned objective leads to the analysis in this paper. In the terminology of approximation theory, the set of propagative plane waves is not a frame for its span (i.e., for the approximation space). In particular, it lacks a so-called lower frame bound, an issue that is connected to the possibility of bounded functions nevertheless yielding large coefficients. Unfortunately, while the theory in [1, 2] allows to identify this problem, it offers no concrete suggestions as to how it can be remedied.

A general principle is that, in the presence of ill-conditioning and with the use of regularization techniques, in order to obtain accurate results in floating-point arithmetic it is no longer sufficient to study best approximation errors. Rather, one is led to study approximation error in relation to coefficient norm, i.e., the norm of the coefficients in the expansion. The former depends solely on the approximation space, but the coefficient norm also depends on its chosen representation (namely plane waves). We formalize this in the notion of a *stable approximation* in Definition 3.1. The corresponding error analysis, based largely on results in [1, 2], allows us to conclude that the set of propagative plane waves does not always yield stable approximations. That is, we can formally state that there exist Helmholtz solutions well approximated in the approximation space which are nevertheless not numerically computable.

Next, we proceed beyond [1, 2] in order to solve the issue. If the approximation space remains unchanged, a lower frame bound can only be established through a change of basis, such as orthogonalization. However, that changes the representation: the solution would no longer

be represented in the simple form of an expansion in plane waves. Enriching the approximation space by evanescent waves seems like a logical alternative. Yet, it is a non-trivial task to identify a suitable set of waves which provably delivers controllable accuracy in combination with stability.

1.4 Main results

Our main result at the continuous level states that any solution u of the Helmholtz equation in the unit disk can be uniquely represented in the form of a continuous superposition of evanescent plane waves, see Theorem 6.7. This integral representation can be seen as a generalization of the classical Herglotz representation, see e.g. [11, 31]. We show that the density v that appears in the integral representation $u = Tv$, which we call Herglotz density, belongs to a weighted L^2 space \mathcal{A} , for which we provide an explicit Hilbert basis. We prove that the integral operator T that maps Herglotz densities to Helmholtz solutions is invertible and bounded, and we name it *Herglotz transform*. This is a strong stability result and similar statements do not hold with propagative waves only. This result implies that the evanescent plane waves are a continuous frame for the space of Helmholtz solutions. While this is stated at the continuous level, such a property paves the way for successful stable discrete expansions.

As a noteworthy corollary, the space of Herglotz densities has the reproducing kernel property, namely point-evaluation functionals are continuous. Moreover, and this is a key point, any point-evaluation functional can be identified with an element of the parametric domain by Riesz identification and maps into an evanescent plane wave under the transform T .

In view of practical implementations, discretizations strategies have been investigated. In this respect, the problem can be seen as the construction of a quadrature rule in the unbounded parametric domain, adapted to the subspace of the Herglotz densities, to approximate Tv . Unfortunately, our setting does not seem to fall within the assumptions of existing results that guarantee the existence of such discretization procedures (e.g. the boundedness assumption of [16, Th. 1.3] is not satisfied).

In spite of this, we are able to propose a numerical scheme which is experimentally shown to exhibit many of the desired properties we are looking for. The starting point is the optimal sampling procedure for weighted least-squares recently described by Cohen and Migliorati [10] (see also [19]). In this work, they consider the problem of the reconstruction of unknown functions in weighted L^2 spaces from a finite number of point values. They consider hierarchical families of finite dimensional subspaces, and advocate to generate independent random samples following an optimal sampling measure. They show that a number of samples scaling log-linearly with respect to the dimension of the reconstruction subspace is enough to recover, in expectation, the best approximation from the collected samples. The underlying key result is a Marcinkiewicz–Zygmund inequality, from which many results of numerical approximation can be deduced [2, 17].

The probability density function according to which the sampling points should be generated is a generalization to the multivariate setting of (the reciprocal of) the Christoffel function (sometimes called spectral function) associated to an orthonormal basis. The appearance of this function is not surprising since it is already ubiquitous in the theory of orthogonal polynomials and associated numerical quadrature rules.

We conjecture that, by applying the sampling strategy in the parametric space \mathcal{A} and exploiting the reproducing kernel property, one can generate suitable sets of sampling functionals to approximate elements in the space of Herglotz densities. Essential to the success of this procedure, we already have at hand an explicit Hilbert basis for the parametric space. This allows, on the one hand, to naturally construct a hierarchical sequence of finite-dimensional subspaces by truncating the Hilbert basis sequence, and, on the other hand, to compute the Christoffel

function. We can therefore generate a set of sampling functionals that approximates well the Herglotz densities. Then, applying the continuous transform T to these approximations gives rise to accurate approximation of the Helmholtz solution in the physical domain as an expansion in terms of evanescent plane waves.

The conjecture is tested numerically, and the results are shown to be in agreement with the expectations. In particular, provided one uses sufficient oversampling and regularization, the resulting approximations are shown to be both controllably accurate and numerically stable. Besides, this procedure provides quasi-optimal approximations in the sense that the number of evanescent plane waves necessary to approximate a given element of a finite-dimensional space scales linearly with the dimension of the subspace.

Finally, we highlight that the approach, although only applicable to the disk for the time being, is very concrete and not difficult to implement in practice. It is very robust with intuitive parameters to provide controllable accuracy. Our own implementation is short and publicly available.

The rigorous analysis of the numerical results obtained using the above approach is not yet complete. In particular, it currently remains an open problem to prove that the approximations constructed in practice have the much desired properties to be at the same time accurate and stable (with bounded coefficients). However, the proven result at the continuous level is a very strong indication that the conjecture is true, and this is further supported by plentiful numerical evidence. Still, such an investigation is the subject of subsequent work.

1.5 Outline of the paper

In Section 2 we start by recalling a number of known results concerning Helmholtz solutions in circular geometries, in particular on the Hilbert basis provided by the so-called circular waves.

Definition 3.1 gives the essential notion of stable approximation for Helmholtz solutions. In Sections 3.2–3.3, we describe a practical sampling-based numerical scheme to compute approximations of Helmholtz solutions that rely on regularized Singular Value Decomposition and oversampling. Corollary 3.3 shows that this scheme guarantees accurate solutions, provided the approximation set has the stable-approximation property.

Section 4 clarifies the issues raised by the use of propagative plane waves in Trefftz schemes, in particular their unstable nature, which is the main assessment that motivated this paper. We emphasize the impossibility of computing accurate approximations with plane waves in computer arithmetic, even using regularization techniques, because of the unavoidable exponential growth of the coefficients, see Theorem 4.3.

Then Section 5 introduces evanescent plane waves, which we propose as a generalization of propagative plane waves that does not suffer from the same numerical instability.

Section 6 is devoted to the introduction (in Definition 6.6) and the analysis of an integral operator $T : \mathcal{A} \rightarrow \mathcal{B}$ that maps the space \mathcal{A} of Herglotz densities defined on a parametric domain Y onto the space \mathcal{B} of Helmholtz solutions on the unit disk B_1 . The main result is Theorem 6.7, which states that this operator is a bounded and invertible integral transform. We also show that evanescent waves constitute a continuous frame and that the parametric space \mathcal{A} is a reproducing kernel Hilbert space.

The results in the continuous setting are the foundation for the numerical recipe that we propose in Section 7. This is based on Conjecture 7.1, which implies that a stable set of evanescent plane waves can be constructed by sampling the parametric domain according to a probability density function equal to the reciprocal of the Christoffel function associated to a hierarchy of finite dimensional spaces.

Several numerical results are provided in Section 8, corroborating our conjecture and supporting the use of evanescent plane waves for the approximation of Helmholtz solutions.

We finally draw some conclusions in Section 9.

2 Helmholtz equation in circular geometry

We first present the setting of the paper and introduce some notations.

2.1 Circular waves

In this paper we only consider circular two-dimensional geometries. Therefore, up to a rescaling of the wavenumber κ and without loss of generality, we assume that the domain is the (open) unit disk, henceforth denoted $B_1 := \{\mathbf{x} \in \mathbb{R}^2 \mid \|\mathbf{x}\| < 1\}$.

The circular geometry enables modal analysis via separation of variables. The *circular waves* are the bounded solutions of the Helmholtz equation in the unit disk that are separable in polar coordinates. They are sometimes also referred to as *Fourier–Bessel functions* or as *Generalized Harmonic Polynomials* [26].

Let us introduce the following κ -dependent scalar product and associated norm: for any $u, v \in H^1(B_1)$,

$$\begin{aligned} (u, v)_{\mathcal{B}} &:= (u, v)_{L^2(B_1)} + \kappa^{-2} (\nabla u, \nabla v)_{L^2(B_1)}, \\ \|u\|_{\mathcal{B}}^2 &:= (u, u)_{\mathcal{B}}. \end{aligned} \quad (2.1)$$

Definition 2.1 (Circular waves). *We define, for any $p \in \mathbb{Z}$*

$$\begin{aligned} \tilde{b}_p(\mathbf{x}) &:= J_p(\kappa r) e^{ip\theta}, \quad \forall \mathbf{x} = (r, \theta) \in B_1, \\ b_p &:= \beta_p \tilde{b}_p, \quad \text{where} \quad \beta_p := \|\tilde{b}_p\|_{\mathcal{B}}^{-1}, \end{aligned} \quad (2.2)$$

and

$$\mathcal{B} := \overline{\text{span}\{b_p\}_{p \in \mathbb{Z}}}^{\|\cdot\|_{\mathcal{B}}} \subsetneq H^1(B_1). \quad (2.3)$$

In this definition, J_p is the usual Bessel function of the first kind [15, Eq. (10.2.2)].

A representation of the real part of some circular waves is given in Figure 1. We will refer to the circular waves with mode number $|p| < \kappa$ as *propagative* modes. The ‘energy’ of such modes is distributed in the bulk of the domain. On the contrary, for $|p| \gg \kappa$, the circular waves are termed *evanescent*. Their ‘energy’ is concentrated near the boundary of the domain. In between, the waves such that $|p| \approx \kappa$ are called *grazing* modes.

Lemma 2.2. *The space $(\mathcal{B}, \|\cdot\|_{\mathcal{B}})$ is a Hilbert space and the family $\{b_p\}_{p \in \mathbb{Z}}$ is a Hilbert basis (i.e. an orthonormal basis):*

$$(b_p, b_q)_{\mathcal{B}} = \delta_{pq}, \quad \forall p, q \in \mathbb{Z}, \quad \text{and} \quad u = \sum_{p \in \mathbb{Z}} (u, b_p)_{\mathcal{B}} b_p, \quad \forall u \in \mathcal{B}. \quad (2.4)$$

Proof. We only need to prove that the family $\{b_p\}_{p \in \mathbb{Z}}$ is orthogonal, which is a consequence of the orthogonality of the complex exponentials $\{\theta \mapsto e^{ip\theta}\}_{p \in \mathbb{Z}}$ on the unit circle ∂B_1 . For $p, q \in \mathbb{Z}$, we have

$$(\tilde{b}_p, \tilde{b}_q)_{L^2(B_1)} = \int_0^1 J_p(\kappa r) J_q(\kappa r) r \, dr \int_0^{2\pi} e^{i(p-q)\theta} \, d\theta = 2\pi \int_0^1 J_p^2(\kappa r) r \, dr \, \delta_{pq}. \quad (2.5)$$

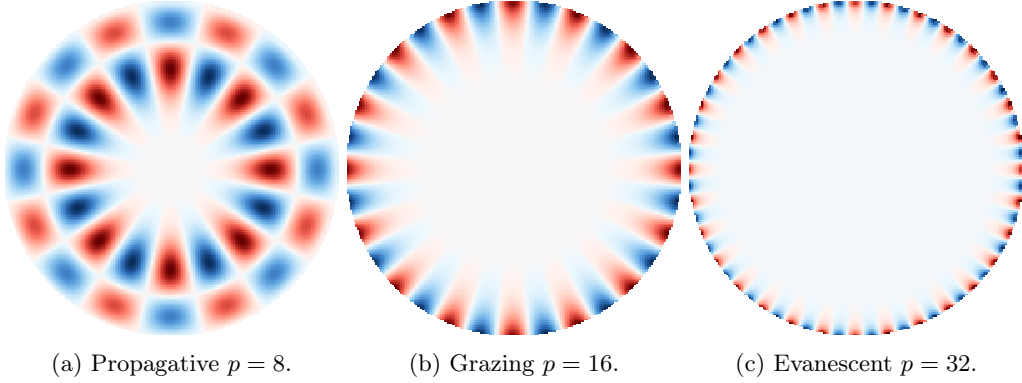


Figure 1: Real part of the circular waves \tilde{b}_p on the disk B_1 for wavenumber $\kappa = 16$.

The orthogonality in $H^1(B_1)$ is easily seen from

$$\begin{aligned} \left(\nabla \tilde{b}_p, \nabla \tilde{b}_q \right)_{L^2(B_1)^2} &= \left(-\Delta \tilde{b}_p, \tilde{b}_q \right)_{L^2(B_1)} + \left(\partial_{\mathbf{n}} \tilde{b}_p, \tilde{b}_q \right)_{L^2(\partial B_1)} \\ &= \kappa^2 \left(\tilde{b}_p, \tilde{b}_q \right)_{L^2(B_1)} + \left(\partial_{\mathbf{n}} \tilde{b}_p, \tilde{b}_q \right)_{L^2(\partial B_1)}, \end{aligned} \quad (2.6)$$

where we denoted by \mathbf{n} the outward unit normal vector and

$$\left(\partial_{\mathbf{n}} \tilde{b}_p, \tilde{b}_q \right)_{L^2(\partial B_1)} = \kappa J'_p(\kappa) J_q(\kappa) \int_0^{2\pi} e^{i(p-q)\theta} d\theta = 2\pi \kappa J'_p(\kappa) J_p(\kappa) \delta_{pq}. \quad (2.7)$$

□

The main reason for introducing circular waves is the possibility to use them to expand any Helmholtz solution on the disk, as we show in the next lemma. Related results for more general domains and different norms are available, see e.g. [20, Sec. 3.1].

Lemma 2.3. *$u \in H^1(B_1)$ satisfies the Helmholtz equation (1.1) if and only if $u \in \mathcal{B}$.*

Proof. It is straightforward to check that any b_p , for $p \in \mathbb{Z}$, is solution to the Helmholtz equation (1.1). The continuity of the Helmholtz operator

$$\mathcal{L} : H^1(B_1) \rightarrow H^{-1}(B_1) = (H_0^1(B_1))^*, \quad (2.8)$$

defined by

$$\langle \mathcal{L}u, v \rangle_{H^{-1} \times H_0^1} := (\nabla u, \nabla v)_{L^2(B_1)} - \kappa^2 (u, v)_{L^2(B_1)}, \quad \forall u \in H^1(B_1), v \in H_0^1(B_1), \quad (2.9)$$

implies that the kernel of \mathcal{L} is a closed subspace of $H^1(B_1)$. From the definition of \mathcal{B} given in (2.3), it follows that

$$\mathcal{B} \subset \ker \mathcal{L} := \{u \in H^1(B_1) \mid \mathcal{L}u = 0\}. \quad (2.10)$$

Conversely, let $u \in H^1(B_1)$ satisfy (1.1) and set $g := \partial_{\mathbf{n}} u - \iota \kappa u \in H^{-1/2}(\partial B_1)$. The Robin trace g can be written

$$g(\theta) = \sum_{p \in \mathbb{Z}} \hat{g}_p e^{ip\theta}, \quad \forall \theta \in [0, 2\pi), \quad \text{with} \quad \sum_{p \in \mathbb{Z}} |\hat{g}_p|^2 (1 + p^2)^{-1/2} < \infty. \quad (2.11)$$

Let $P \geq 0$, and set $g_P(\theta) := \sum_{|p| < P} \hat{g}_p e^{ip\theta}$, for $\theta \in [0, 2\pi)$. Then there exists a unique $u_P \in \text{span}\{b_p\}_{|p| < P}$, such that $g_P = \partial_{\mathbf{n}} u_P - \imath \kappa u_P$, namely $u_P = \sum_{|p| < P} \hat{g}_p (\kappa \beta_p (J'_p(\kappa) - \imath J_p(\kappa)))^{-1} b_p$ (the term $J'_p(\kappa) - \imath J_p(\kappa)$ at the denominator is non-zero because of [15, Eq. (10.21.2)]). The well-posedness of the problem: find $v \in H^1(B_1)$ such that

$$-\Delta v - \kappa^2 v = 0, \quad \text{in } B_1, \quad \text{and} \quad \partial_{\mathbf{n}} v - \imath \kappa v = h, \quad \text{on } \partial B_1, \quad (2.12)$$

for $h \in H^{-1/2}(\partial B_1)$ [26, Prop. 8.1.3], implies that there exists a constant $C > 0$, independent of P , such that

$$\|u - u_P\|_{\mathcal{B}} \leq C \|g - g_P\|_{H^{-1/2}(\partial B_1)}. \quad (2.13)$$

Letting P tend to infinity, we obtain that $u \in \mathcal{B}$. \square

The circular (and spherical) waves have been used in many Trefftz schemes, see [20, Sec. 3.1] and the references therein. An interesting feature of such waves is that the approximation sets are naturally hierarchical.

2.2 Asymptotics of normalization coefficients

The coefficients β_p grow super-exponentially with $|p|$ after a pre-asymptotic regime up to $|p| \approx \kappa$. The precise asymptotic behavior is given by the following lemma.

Lemma 2.4. *We have for all $p \in \mathbb{Z}$*

$$\beta_p = \left(2\pi [J_p^2(\kappa) - J_{p-1}(\kappa)J_{p+1}(\kappa) + J'_p(\kappa)J_p(\kappa)/\kappa]\right)^{-1/2}, \quad (2.14)$$

and

$$\beta_p \sim \kappa \left(\frac{2}{e\kappa}\right)^{|p|} |p|^{|p|}, \quad \text{as } |p| \rightarrow +\infty. \quad (2.15)$$

Proof. The explicit expression for β_p can be deduced by integration by parts as in the proof of Lemma 2.2. From (2.6), the explicit expression for the boundary term (2.7) and [15, Eq. (10.22.5)]

$$\|\tilde{b}_p\|_{L^2(B_1)}^2 = 2\pi \int_0^1 J_p^2(\kappa r) r \, dr = \pi (J_p^2(\kappa) - J_{p-1}(\kappa)J_{p+1}(\kappa)), \quad (2.16)$$

we readily deduce (2.14).

The proof for the asymptotic behavior consists in showing that we have

$$\begin{aligned} \|\tilde{b}_p\|_{L^2(\partial B_1)} &\sim \left(\frac{e\kappa}{2}\right)^{|p|} |p|^{-(|p|+1/2)}, \\ \|\tilde{b}_p\|_{L^2(B_1)} &\sim \frac{1}{\sqrt{2}} \left(\frac{e\kappa}{2}\right)^{|p|} |p|^{-(|p|+1)}, \quad \text{as } |p| \rightarrow +\infty. \\ \|\tilde{b}_p\|_{\mathcal{B}} &\sim \kappa^{-1} \left(\frac{e\kappa}{2}\right)^{|p|} |p|^{-|p|}, \end{aligned} \quad (2.17)$$

First we remark that for any $p \in \mathbb{Z}$, $J_{-p} = (-1)^p J_p$ from [15, Eq. (10.4.1)]. Therefore, the asymptotic behavior will not depend on the sign of p , and we suppose $p > 0$ in the following.

We start with the trace: from the definition (2.2) of \tilde{b}_p we immediately have $\|\tilde{b}_p\|_{L^2(\partial B_1)}^2 = 2\pi J_p^2(\kappa)$, and from [15, Eq. (10.19.1)], namely

$$J_\nu(z) \sim \frac{1}{\sqrt{2\pi\nu}} \left(\frac{ez}{2\nu}\right)^\nu, \quad \text{as } \nu \rightarrow +\infty, \quad z \neq 0, \quad (2.18)$$

the first result in (2.17) follows.

We now consider the $L^2(B_1)$ norm. From (2.16) and (2.18), we get as $p \rightarrow +\infty$

$$\|\tilde{b}_p\|_{L^2(B_1)}^2 \sim \frac{1}{2} \left(\frac{e\kappa}{2}\right)^{2p} p^{-(2p+1)} \left[1 - \frac{p^{2p+1}}{(p-1)^{p-1/2}(p+1)^{p+3/2}}\right], \quad (2.19)$$

and it is readily checked that the term inside the square brackets is equivalent to p^{-1} at infinity.

We now consider the κ -weighted $H^1(B_1)$ norm (2.1). We need to study the asymptotic of the boundary term (2.7). From [15, Eq. (10.6.1)]

$$\left(\partial_n \tilde{b}_p, \tilde{b}_p\right)_{L^2(\partial B_1)} = 2\pi\kappa J'_p(\kappa) J_p(\kappa) = \pi\kappa (J_{p-1}(\kappa) - J_{p+1}(\kappa)) J_p(\kappa). \quad (2.20)$$

From (2.18), we get as $p \rightarrow +\infty$

$$\left(\partial_n \tilde{b}_p, \tilde{b}_p\right)_{L^2(\partial B_1)} \sim \frac{\kappa}{2} \left(\frac{e\kappa}{2}\right)^{2p} p^{-(2p+1)} \left[\frac{2}{e\kappa} \frac{p^{p+1/2}}{(p-1)^{p-1/2}} - \frac{e\kappa}{2} \frac{p^{p+1/2}}{(p+1)^{p+3/2}}\right], \quad (2.21)$$

and it is readily checked that the first term inside the square brackets is dominant and equivalent to $\frac{2}{\kappa}p$ at infinity. Thus, the dominant term in (2.6) in the limit $p \rightarrow \infty$ is the boundary term. \square

Remark 2.5. We chose to normalize the circular waves using the rather natural \mathcal{B} norm. Other norms considered in the above proof modify the exponential growth of the normalization constants only by some moderate powers of $|p|$, see (2.17). Similarly, if one chooses the L^∞ -norm on the boundary, we have

$$\|\tilde{b}_p\|_{L^\infty(\partial B_1)} = |J_p(\kappa)| \sim \frac{1}{\sqrt{2\pi}} \left(\frac{e\kappa}{2}\right)^{|p|} |p|^{-(|p|+1/2)}, \quad \text{as } |p| \rightarrow +\infty. \quad (2.22)$$

3 Stable numerical approximation

The purpose of this section is to explain the crucial notion of stability when computing numerical approximations in the form of series expansions. Our approach builds on the results in [1, 2]. We also describe the practical procedure, a regularized sampling method, that we use to investigate the existence of stable numerical approximations of Helmholtz solutions in this paper.

3.1 The notion of stable approximation

Let us consider a sequence of finite approximation sets in \mathcal{B}

$$\Phi := \{\Phi_k\}_{k \in \mathbb{N}} \quad \text{where} \quad \Phi_k := \{\phi_{k,l}\}_l, \quad \forall k \in \mathbb{N}, \quad (3.1)$$

and for each k, l , $\phi_{k,l} \in \mathcal{B}$ is a solution of the Helmholtz equation (1.1) in the unit disk. These sets need not be nested.

Associated to any set Φ_k for some $k \in \mathbb{N}$, we define the synthesis operator

$$\begin{aligned} \mathcal{T}_{\Phi_k} : \mathbb{C}^{|\Phi_k|} &\rightarrow \mathcal{B}, \\ \mu &= \{\mu_l\}_l \mapsto \sum_l \mu_l \phi_{k,l}. \end{aligned} \quad (3.2)$$

We are now ready to define a notion of *stable approximation*, which is at the heart of this paper.

Definition 3.1 (Stable approximation). *The sequence Φ of approximation sets (3.1) is said to be a stable approximation for \mathcal{B} if, for any tolerance $\eta > 0$, there exist a stability exponent $s \geq 0$ and a stability constant $C_{\text{stb}} \geq 0$ such that*

$$\forall u \in \mathcal{B}, \exists \Phi_k \in \Phi, \mu \in \mathbb{C}^{|\Phi_k|} \quad \text{such that} \quad \begin{cases} \|u - \mathcal{T}_{\Phi_k} \mu\|_{\mathcal{B}} \leq \eta \|u\|_{\mathcal{B}} & \text{and} \\ \|\mu\|_{\ell^2} \leq C_{\text{stb}} |\Phi_k|^s \|u\|_{\mathcal{B}}. \end{cases} \quad (3.3)$$

Having a sequence of stable approximation sets means that one can approximate any Helmholtz solution to a given accuracy in the form of a finite expansion $\mathcal{T}_{\Phi_k} \mu$ where the coefficients μ have bounded ℓ^2 -norm, up to some algebraic growth in the number of terms in the expansion. The stability exponent $s \geq 0$ of a stable approximation sequence controls the growth of the coefficient norm: the smaller s the more stable the sequence.

Since algebraic growth of the coefficient norm is allowed, the choice of the discrete ℓ^2 -norm in (3.3) in the above definition is arbitrary. In fact, the boundedness of the coefficients can be measured in any discrete ℓ^p norm, which are all equivalent as expressed by the Hölder inequality: for any $n \in \mathbb{N}$ and $1 \leq q \leq p$,

$$\|\mu\|_{\ell^p} \leq \|\mu\|_{\ell^q} \leq n^{\frac{1}{q} - \frac{1}{p}} \|\mu\|_{\ell^p}, \quad \forall \mu \in \mathbb{C}^n. \quad (3.4)$$

Choosing a different discrete norm in (3.3) can increase the stability exponent s (up to $s + 1/2$ for the ℓ^1 -norm).

We shall present in the following two examples of approximations sets of the type of (3.1): propagative plane waves in (4.3) and evanescent plane waves in (7.17). They exhibit different stability properties, see Theorem 4.3 and Section 7.3.

3.2 Boundary sampling method

Let us explain now how we compute the coefficients in practice. For simplicity, our strategy is of sampling type, following [22]. All the numerical results obtained in this paper are obtained using the method described below.

Let us introduce a ‘trace operator’ γ , namely a (continuous) linear operator defined on $H^1(B_1)$ such that the problem: find $u \in H^1(B_1)$ such that

$$-\Delta u - \kappa^2 u = 0, \quad \text{in } B_1, \quad \text{and} \quad \gamma u = g, \quad \text{on } \partial B_1, \quad (3.5)$$

for some suitable boundary data g , is well-posed. Examples of such a trace operator γ are: the Dirichlet trace operator, extension to $H^1(B_1)$ of $u \mapsto u|_{\partial B_1}$, when κ^2 is not an eigenvalue of the Dirichlet Laplacian; the Neumann trace operator, extension to $H^1(B_1)$ of $u \mapsto \partial_{\mathbf{n}} u$, when κ^2 is not an eigenvalue of the Neumann Laplacian; the Robin trace operator, extension to $H^1(B_1)$ of $u \mapsto \partial_{\mathbf{n}} u - \imath \kappa u|_{\partial B_1}$ (without assumptions on the wavenumber κ).

In this paper, and in all our numerical experiments, we aim at reconstructing a solution $u \in \mathcal{B}$ having access to its trace γu on the boundary for such a ‘good’ trace operator γ . For simplicity, we use the Dirichlet trace operator and therefore assume that κ^2 is away from the eigenvalues of the Dirichlet Laplacian. Further we will assume that $u \in \mathcal{B} \cap C^0(\overline{B_1})$, so that it makes sense to consider point evaluations of the Dirichlet trace.

The reconstruction process is *not* the main subject of the paper (which concerns the existence of stable approximation set sequences and their computation) and we stress that we make these two assumptions mainly for convenience and definiteness (in particular for the numerical experiments). One can consider alternative reconstruction procedures using other types of data, such as point evaluation in the bulk of the domain or by taking inner product of the solution

with suitable test functions. See [8] for a more general discussion on the subject of reconstructing Helmholtz solutions from point evaluations. The regularity assumption $u \in C^0(\overline{B_1})$ can be lifted by using continuous least-squares formulations of the problem (by which we mean taking inner products of the trace of the solution with the elements of the approximation sets).

Let $u \in \mathcal{B} \cap C^0(\overline{B_1})$ be the target of the approximation problem. We look for a set of coefficients $\xi \in \mathbb{C}^{|\Phi_k|}$ for a given approximation set Φ_k (introduced in (3.1)) such that $\mathcal{T}_{\Phi_k} \xi \approx u$. We also assume that for any l , $\phi_{k,l} \in \mathcal{B} \cap C^0(\overline{B_1})$. Define the set of $S \geq |\Phi_k|$ sampling points $\{\mathbf{x}_s\}_{s=1}^S$ on the unit circle ($|\mathbf{x}_s| = 1$) parametrized by the angle

$$\theta_s = \frac{2\pi s}{S}, \quad 1 \leq s \leq S. \quad (3.6)$$

Let us introduce the matrix $A = (A_{s,l})_{s,l} \in \mathbb{C}^{S \times |\Phi_k|}$ and the vector $\mathbf{b} = (\mathbf{b}_s)_s \in \mathbb{C}^S$ such that

$$A_{s,l} = \phi_{k,l}(\mathbf{x}_s), \quad \mathbf{b}_s = (\gamma u)(\mathbf{x}_s), \quad 1 \leq l \leq |\Phi_k|, \quad 1 \leq s \leq S. \quad (3.7)$$

The sampling method then consists in approximately solving the following possibly overdetermined linear system

$$A\xi = \mathbf{b}. \quad (3.8)$$

3.3 Regularization

It often happens that the matrix A is ill-conditioned (see Section 4.3). In finite precision arithmetic, severe ill-conditioning may prevent us from obtaining accurate solutions. However, the type of ill-conditioning encountered here is benign if it arises only from the redundancy of the approximating functions. In that case, the ill-conditioning is associated with the numerical non-uniqueness of the coefficients in an expansion, yet all expansions may approximate the solution to similar accuracy. If among those expansions there exist some with small coefficient norms, then it is possible to mitigate such ill-conditioning using regularization techniques, as explained in [1], which we describe now. Alternative techniques to curb ill-conditioning can be found in the literature, see [3] where a suitable change of basis is used and works well for circular geometries, and [12] which uses orthogonalization techniques. These techniques are effective precisely when ill-conditioning stems from redundancy.

To obtain a solution even in the presence of ill-conditioning, we rely on the conjugation of oversampling and regularization techniques developed in [1, 2]. Similar techniques in the context of Trefftz methods are also the main subject of [4, 22].

The first step is to compute the Singular Value Decomposition (SVD) of the matrix A , namely

$$A = U\Sigma V^*. \quad (3.9)$$

Let us denote by $(\sigma_m)_m$ for $m = 1, \dots, |\Phi_k|$ the singular values of A , assumed to be sorted in descending order. For notational clarity, the largest singular value is renamed $\sigma_{\max} := \sigma_1$. Then, the regularization amounts to trimming the tail of *relatively* small singular values, which are approximated by zero. Let $\epsilon \in (0, 1]$ be a chosen threshold, we denote by Σ_ϵ the approximation of the diagonal matrix Σ where all diagonal elements σ_m such that $\sigma_m < \epsilon\sigma_{\max}$ are replaced by zero. This leads to the approximate factorization $U\Sigma_\epsilon V$ of the matrix A . An approximate solution to (3.8) is then obtained by

$$\xi_{S,\epsilon} := V\Sigma_\epsilon^\dagger U^* \mathbf{b}. \quad (3.10)$$

Here Σ_ϵ^\dagger denotes the pseudo-inverse of the matrix Σ_ϵ , namely the diagonal matrix with $(\Sigma_\epsilon^\dagger)_{j,j} = (\Sigma_{j,j})^{-1}$ if $\Sigma_{j,j} \geq \epsilon\sigma_{\max}$ and $(\Sigma_\epsilon^\dagger)_{j,j} = 0$ otherwise. Robust computation of $\xi_{S,\epsilon}$ requires to compute the right-hand-side of (3.10) from right to left, namely $\xi_{S,\epsilon} := V(\Sigma_\epsilon^\dagger(U^* \mathbf{b}))$, in order to avoid mixing small and large values on the diagonal of Σ_ϵ^\dagger .

3.4 Error estimates for the sampling method with regularization

With the regularization technique described above together with *oversampling*, i.e., S larger than $|\Phi_k|$, accurate approximations can be effectively computed, provided the set sequence is a stable approximation in the sense of Definition 3.1. This broad statement is the main message of [1, 2], see [1, Th. 5.3] and [2, Th. 1.3 and 3.7], and is the starting point of our quest of stable approximation sets for the solutions of the Helmholtz equation.

More precisely, we have the following proposition, which is a rewording of [2, Th. 3.7] from the context of *generalized sampling* to our setting, with the notations just introduced.

Proposition 3.2. *Let γ be the Dirichlet trace operator and $u \in \mathcal{B} \cap C^0(\overline{B_1})$. Given some approximation set Φ_k ($k \in \mathbb{N}$ fixed) such that for any l , $\phi_{k,l} \in \mathcal{B} \cap C^0(\overline{B_1})$; a sampling set of size $S \in \mathbb{N}$ as described in (3.6) and some regularization parameter $\epsilon \in (0, 1]$, we consider the approximate solution of the linear system (3.8), namely $\xi_{S,\epsilon} \in \mathbb{C}^{|\Phi_k|}$ as defined in (3.10). If S is sufficiently large, then*

$$\|\gamma(u - \mathcal{T}_{\Phi_k} \xi_{S,\epsilon})\|_{L^2(\partial B_1)} \leq \inf_{\mu \in \mathbb{C}^{|\Phi_k|}} \left((1 + 2\sqrt{\pi S}) \|\gamma(u - \mathcal{T}_{\Phi_k} \mu)\|_{L^2(\partial B_1)} + \epsilon \sigma_{\max} \|\mu\|_{\ell^2} \right). \quad (3.11)$$

Moreover, if κ^2 is not an eigenvalue of the Dirichlet Laplacian in B_1 , for a constant C_{err} independent of u , Φ_k and S ,

$$\|u - \mathcal{T}_{\Phi_k} \xi_{S,\epsilon}\|_{L^2(B_1)} \leq C_{\text{err}} \inf_{\mu \in \mathbb{C}^{|\Phi_k|}} \left(\sqrt{S} \|u - \mathcal{T}_{\Phi_k} \mu\|_{\mathcal{B}} + \epsilon \sigma_{\max} \|\mu\|_{\ell^2} \right). \quad (3.12)$$

Proof. The proof consists in showing that we satisfy the assumptions of more general results that can be found in [2] in the context of function approximation with regularization using generalized sampling. These general results involve unknown constants – denoted $\kappa_{M,N}^\epsilon$ and $\lambda_{M,N}^\epsilon$ in [2] – and a non-standard discrete norm – denoted as the M -norm in [2] – which relate to the choice of sampling functionals. In contrast, (3.11)–(3.12) involve only standard norms. The main point of the proposition is that, for sufficiently large S and owing to a judicious choice of normalization, the discrete M -norm is equivalent to a continuous norm and the unknown constants simply tend to 1, hence they disappear from the expressions.

The above-mentioned norm equivalence is expressed by the so-called Marcinkiewicz–Zygmund condition, given by [2, Eq. (3.2)]. The regularity assumption for u and Φ_k , which are assumed in $\mathcal{B} \cap C^0(\overline{B_1})$, allows to have well-defined pointwise evaluations of their image by the Dirichlet trace operator γ on the boundary ∂B_1 . Recall that the sampling nodes $\{\mathbf{x}_s\}_s$ are defined in (3.6). For any $v \in \mathcal{B} \cap C^0(\overline{B_1})$,

$$\lim_{S \rightarrow +\infty} \frac{1}{2\pi S} \sum_{s=1}^S |(\gamma v)(\mathbf{x}_s)|^2 = \|\gamma v\|_{L^2(\partial B_1)}^2. \quad (3.13)$$

The argument of the limit in the left-hand-side is a Riemann sum approximant of the right-hand-side. A similar argument is developed in [2, Ex. 3.3] (note that $A' = B' = 1$ in the notations of [2]).

The norm equivalence (3.13) implies by [2, Th. 3.7 and Prop. 3.10] that

$$\|\gamma(u - \mathcal{T}_{\Phi_k} \xi_{S,\epsilon})\|_{L^2(\partial B_1)} \leq \inf_{\mu \in \mathbb{C}^{|\Phi_k|}} \left(\|\gamma(u - \mathcal{T}_{\Phi_k} \mu)\|_{L^2(\partial B_1)} + \|A\mu - \mathbf{b}\|_{\ell^2} + \epsilon \sigma_{\max} \|\mu\|_{\ell^2} \right). \quad (3.14)$$

The introduction of the largest singular value σ_{\max} of the matrix A compared to [2, Th. 3.7] comes from the fact that we perform a relative truncation of the singular values for the regularization.

Moreover, Equation (3.13) also implies that for any $\boldsymbol{\mu} \in \mathbb{C}^{|\Phi_k|}$ there exists S sufficiently large such that

$$\frac{1}{2\pi S} \|A\boldsymbol{\mu} - \mathbf{b}\|_{\ell^2}^2 = \frac{1}{2\pi S} \sum_{s=1}^S |\gamma(u - \mathcal{T}_{\Phi_k}\boldsymbol{\mu})(\mathbf{x}_s)|^2 \leq 2\|\gamma(u - \mathcal{T}_{\Phi_k}\boldsymbol{\mu})\|_{L^2(\partial B_1)}^2. \quad (3.15)$$

The coefficient 2 above could be replaced by any number strictly larger than 1, the value 2 was chosen for simplicity. Since $\boldsymbol{\mu}$ varies in a finite dimensional space, the number of sampling points S for which the above estimate holds true can be chosen independently of $\boldsymbol{\mu}$ varying in $\mathbb{C}^{|\Phi_k|}$. Combining the bounds (3.14)–(3.15) we get the error estimate (3.11).

In order to show (3.12), note first that the continuity of the trace operator γ from \mathcal{B} to $L^2(\partial B_1)$ allows to write, for any $\boldsymbol{\mu} \in \mathbb{C}^{|\Phi_k|}$,

$$\|\gamma(u - \mathcal{T}_{\Phi_k}\boldsymbol{\mu})\|_{L^2(\partial B_1)} \leq \|\gamma\| \|u - \mathcal{T}_{\Phi_k}\boldsymbol{\mu}\|_{\mathcal{B}}. \quad (3.16)$$

It remains to bound the $L^2(B_1)$ of $u - \mathcal{T}_{\Phi_k}\boldsymbol{\xi}_{S,\epsilon}$, by the $L^2(\partial B_1)$ norm of its trace. Let $\{\hat{e}_p\}_{p \in \mathbb{Z}}$ be the coefficients of $e := u - \mathcal{T}_{\Phi_k}\boldsymbol{\xi}_{S,\epsilon}$, in the Hilbert basis $\{b_p\}_{p \in \mathbb{Z}}$. From the asymptotics (2.17), we have

$$\|e\|_{\mathcal{B}}^2 = \sum_{p \in \mathbb{Z}} |\hat{e}_p|^2, \quad \|e\|_{L^2(B_1)}^2 = \sum_{p \in \mathbb{Z}} c_p^{(1)} \frac{|\hat{e}_p|^2}{1 + p^2}, \quad \|e\|_{L^2(\partial B_1)}^2 = \sum_{p \in \mathbb{Z}} c_p^{(2)} \frac{|\hat{e}_p|^2}{\sqrt{1 + p^2}}, \quad (3.17)$$

where we introduced two sequences of strictly positive constants $\{c_p^{(1)}\}_{p \in \mathbb{Z}}$ and $\{c_p^{(2)}\}_{p \in \mathbb{Z}}$ both bounded below and above, and independent of $u - \mathcal{T}_{\Phi_k}\boldsymbol{\xi}_{S,\epsilon}$. The fact that $\{c_p^{(2)}\}_{p \in \mathbb{Z}}$ is bounded below follows from the fact that κ^2 is not a Dirichlet eigenvalue. We derive (3.12) from this remark and (3.13). \square

Proposition 3.2 shows that having stable approximation sets in the sense of Definition 3.1 is a sufficient condition for the accurate reconstruction of a Helmholtz solution from its samples on the boundary of the disk, provided one uses enough sampling points S and a sufficiently small regularization parameter ϵ . More precisely, we have the following corollary.

Corollary 3.3. *Let $\delta > 0$. We assume to have a sequence of approximation sets $\{\Phi_k\}_{k \in \mathbb{N}}$ that is stable in the sense of Definition 3.1. Assume also that κ^2 is not a Dirichlet eigenvalue in B_1 . Then,*

$$\forall u \in \mathcal{B} \cap C^0(\overline{B_1}), \exists \Phi_k, S \in \mathbb{N}, \epsilon \in (0, 1], \text{ such that } \|u - \mathcal{T}_{\Phi_k}\boldsymbol{\xi}_{S,\epsilon}\|_{L^2(B_1)} \leq \delta \|u\|_{\mathcal{B}}, \quad (3.18)$$

where $\boldsymbol{\xi}_{S,\epsilon} \in \mathbb{C}^{|\Phi_k|}$ is defined in (3.10). Moreover, we can take the regularization parameter ϵ as large as

$$\epsilon = \frac{\delta}{2C_{\text{err}}\sigma_{\text{max}}C_{\text{stb}}|\Phi_k|^s}. \quad (3.19)$$

Proof. Let $\eta > 0$ and $u \in \mathcal{B} \cap C^0(\overline{B_1})$. The stability assumption implies that there exists Φ_k and $\boldsymbol{\mu} \in \mathbb{C}^{|\Phi_k|}$ such that

$$\|u - \mathcal{T}_{\Phi_k}\boldsymbol{\mu}\|_{\mathcal{B}} \leq \eta \|u\|_{\mathcal{B}} \quad \text{and} \quad \|\boldsymbol{\mu}\|_{\ell^2} \leq C_{\text{stb}}|\Phi_k|^s \|u\|_{\mathcal{B}}. \quad (3.20)$$

Then Proposition 3.2 implies the existence of $S \in \mathbb{N}$ such that for this particular $\boldsymbol{\mu}$ we have

$$\|u - \mathcal{T}_{\Phi_k}\boldsymbol{\xi}_{S,\epsilon}\|_{L^2(B_1)} \leq C_{\text{err}} \left(\sqrt{S} \|u - \mathcal{T}_{\Phi_k}\boldsymbol{\mu}\|_{\mathcal{B}} + \epsilon \sigma_{\text{max}} \|\boldsymbol{\mu}\|_{\ell^2} \right) \leq C_{\text{err}} \left(\eta \sqrt{S} + \epsilon \sigma_{\text{max}} C_{\text{stb}} |\Phi_k|^s \right) \|u\|_{\mathcal{B}}. \quad (3.21)$$

It remains to choose the free parameters $\eta > 0$ and $\epsilon \in (0, 1]$ small enough to get the right-hand-side below δ , namely $\eta \leq \frac{\delta}{2\sqrt{S}C_{\text{err}}}$ and ϵ as in (3.19). \square

The point of Corollary 3.3 is not that for any solution u there exists a coefficient vector $\boldsymbol{\mu}$ such that $\mathcal{T}_{\Phi_k} \boldsymbol{\mu}$ is an accurate approximation of u , but rather that the vector $\boldsymbol{\xi}_{S,\epsilon} \in \mathbb{C}^{|\Phi_k|}$ computed using the regularized SVD (3.10) provides an accurate approximation $\mathcal{T}_{\Phi_k} \boldsymbol{\xi}_{S,\epsilon}$ of u . Besides, the numerical computation of $\boldsymbol{\xi}_{S,\epsilon}$ with the SVD and formula (3.10) is stable in floating-point arithmetic, if ϵ is larger than machine precision, which is a reasonable assumption considering (3.19). Thus, the error bounds on $u - \mathcal{T}_{\Phi_k} \boldsymbol{\xi}_{S,\epsilon}$ that we just proved carry over to the solution of the sampling method computed in computer arithmetic. This is in contrast with the classical theory for the approximation by propagative plane waves, e.g. [27], which provides rigorous best-approximation error bounds that often can not be attained numerically, precisely because accurate approximations require large coefficients and cancellation, so exact-arithmetic results are not reflected by floating-point computations.

The assumption on the eigenvalues in Corollary 3.3 can be lifted if in (3.18) the $L^2(B_1)$ norm is replaced by $L^2(\partial B_1)$. Moreover, in this case, the constant C_{err} at the right-hand side of (3.19) can be dropped.

The largest singular value σ_{\max} of the matrix A appears in the above results: in our numerical experiments σ_{\max} is moderate, see Figures 4 and 10.

In the following discussion, it will be convenient to measure the error of the approximation as given by the following relative residual

$$\mathcal{E} = \mathcal{E}(u, \Phi_k, S, \epsilon) := \frac{\|A\boldsymbol{\xi}_{S,\epsilon} - \mathbf{b}\|_{\ell^2}}{\|\mathbf{b}\|_{\ell^2}}, \quad (3.22)$$

where $\boldsymbol{\xi}_{S,\epsilon}$ is the solution (3.10) of the regularized linear system. Arguing as in the proof of Proposition 3.2, for sufficiently large S , the quantity \mathcal{E} satisfies (for a constant \tilde{C} independent of u, Φ_k, S)

$$\|u - \mathcal{T}_{\Phi_k} \boldsymbol{\xi}_{S,\epsilon}\|_{L^2(B_1)} \leq \tilde{C} \|u\|_{\mathcal{B}} \mathcal{E}. \quad (3.23)$$

4 Instability of propagative plane wave sets

The purpose of this section is to present the pitfalls encountered when using *propagative* plane waves to approximate Helmholtz solutions in the unit disk. In particular, as we prove next, propagative plane waves with equispaced angles fail to yield stable approximations. Yet, approximations of Helmholtz solutions using propagative plane wave expansions are the main ingredient of many Trefftz schemes.

4.1 Propagative plane waves

We introduce now the notion of *propagative plane wave*. The adjective *propagative* is not customary in the literature, but serves to distinguish the following definition with the notion of *evanescent* plane waves that will be introduced later (see Definition 5.1).

Definition 4.1 (Propagative plane wave). *For any angle $\varphi \in [0, 2\pi)$, we let*

$$\phi_{\varphi}(\mathbf{x}) := e^{i\kappa \mathbf{d}(\varphi) \cdot \mathbf{x}}, \quad \forall \mathbf{x} \in \mathbb{R}^2, \quad (4.1)$$

where the propagative direction of the wave is given by

$$\mathbf{d}(\varphi) := (\cos \varphi, \sin \varphi) \in \mathbb{R}^2. \quad (4.2)$$

It is immediate to check that any propagative plane wave satisfies the homogeneous Helmholtz equation (1.1) since $\mathbf{d}(\varphi) \cdot \mathbf{d}(\varphi) = 1$ for any angle $\varphi \in [0, 2\pi)$.

Propagative plane waves are a common choice in Trefftz schemes, see [20, Sec. 3.2] and the references therein. In 2D, isotropic approximations are obtained by using equispaced angles: for some $M \in \mathbb{N}$, the approximation set is defined as

$$\Phi_M := \{M^{-1/2} \phi_{\varphi_{M,m}}\}_{m=1}^M, \quad \text{where} \quad \varphi_{M,m} := \frac{2\pi m}{M}, \quad 1 \leq m \leq M. \quad (4.3)$$

In contrast to circular waves, the approximation sets based on such propagative plane waves are in general not hierarchical. Plane waves spaces have been studied in the literature, in particular explicit hp -estimates in suitable Sobolev semi-norms are available for general domains, see [27, Th. 5.2 and 5.3]. These results ensure more than exponential convergence (with respect to the number of plane waves used) of the approximation of homogeneous Helmholtz solutions by a finite superposition of (propagative) plane waves. Therefore, at least in principle, propagative plane waves are well-suited for Trefftz approximations.

Let us state an essential identity that is ubiquitous in the following analysis. The *Jacobi–Anger identity* provides a link between plane waves and circular waves, see [15, Eq. (10.12.1)] and [15, Eq. (10.11.1)]. For any $\mathbf{x} = (r, \theta) \in B_1$ and $\varphi \in [0, 2\pi)$, we have

$$\phi_\varphi(r, \theta) = e^{i\kappa \mathbf{d}(\varphi) \cdot \mathbf{x}} = \sum_{p \in \mathbb{Z}} i^p J_p(\kappa r) e^{ip(\theta - \varphi)}. \quad (4.4)$$

4.2 Herglotz representation

We now recall the so-called *Herglotz functions*, defined, for any $v \in L^2([0, 2\pi])$, as

$$u_v(\mathbf{x}) := \int_0^{2\pi} v(\varphi) \phi_\varphi(\mathbf{x}) \, d\varphi, \quad \forall \mathbf{x} \in \mathbb{R}^2, \quad (4.5)$$

see [11, Eq. (1.1)], [31, Eq. (6)] and [13, Def. 3.18]. Such an expression is termed *Herglotz representation*. The function v is called Herglotz kernel or density.

These functions $u_v \in C^\infty(\mathbb{R}^2)$ are entire solutions of the Helmholtz equation and can be seen as a continuous superposition of propagative plane waves, weighted according to v . To see this, let $v \in L^2([0, 2\pi])$, which we write as a Fourier expansion

$$v(\varphi) = \frac{1}{2\pi} \sum_{p \in \mathbb{Z}} \hat{v}_p e^{ip\varphi}, \quad \forall \varphi \in [0, 2\pi], \quad (4.6)$$

for a sequence of coefficients $(\hat{v}_p)_{p \in \mathbb{Z}} \in \ell^2(\mathbb{Z})$. Then, plugging this expression into (4.5) and using the Jacobi–Anger expansion (4.4) together with the orthogonality of the complex exponentials $\{\theta \mapsto e^{ip\theta}\}_{p \in \mathbb{Z}}$, we obtain, for any $\mathbf{x} = (r, \theta) \in \mathbb{R}^2$,

$$u_v(\mathbf{x}) = \int_0^{2\pi} v(\varphi) \phi_\varphi(\mathbf{x}) \, d\varphi = \sum_{p \in \mathbb{Z}} i^p \hat{v}_p J_p(\kappa r) e^{ip\theta} = \sum_{p \in \mathbb{Z}} \frac{i^p \hat{v}_p}{\beta_p} b_p(\mathbf{x}). \quad (4.7)$$

It is readily seen that u_v belongs to \mathcal{B} , thanks to the super-exponential growth of the coefficients $\{\beta_p\}_{p \in \mathbb{Z}}$ shown in Lemma 2.4.

Conversely, several solutions of the Helmholtz equation can *not* be represented in the form (4.5) for any $v \in L^2([0, 2\pi])$. For any sequence $(\hat{u}_p)_{p \in \mathbb{Z}} \in \ell^2(\mathbb{Z})$, the function $u = \sum_{p \in \mathbb{Z}} \hat{u}_p b_p$ belongs to \mathcal{B} , because $(\hat{u}_p)_{p \in \mathbb{Z}} \in \ell^2(\mathbb{Z})$ is a Hilbert basis. If this u admits a Herglotz representation

in the form (4.5) then the coefficients $\{\hat{v}_p\}_{p \in \mathbb{Z}}$ of the Fourier expansion (4.6) of the density v satisfy the relation $\hat{v}_p = i^{-p} \beta_p \hat{u}_p$ for all $p \in \mathbb{Z}$. For v to belong to $L^2([0, 2\pi])$, these coefficients would need to belong to $\ell^2(\mathbb{Z})$. This is only possible if the coefficients $\{\hat{u}_p\}_{p \in \mathbb{Z}}$ decay super-exponentially, to compensate for the growth of $\{\beta_p\}_{p \in \mathbb{Z}}$, again by Lemma (2.4). For instance, the propagative plane waves themselves are not Herglotz functions, because their Fourier coefficients do not decay sufficiently fast, as can be readily seen from the Jacobi–Anger identity (4.4) (in particular, for a propagative plane wave $|i^{-p} \beta_p \hat{u}_p| = 1$ for all p). In fact, the suitable density v for propagative plane waves would need to be a generalized function, the Dirac distribution.

4.3 Propagative plane waves do not give stable approximations

We shall now investigate a model approximation problem to exemplify the numerical issues posed by propagative plane wave expansions. Let us consider the particular (but important) case of the approximation of a circular wave b_p for some $p \in \mathbb{Z}$ by the sequence of approximation sets of propagative plane waves defined in (4.3). It is shown that the two conditions in (3.3), namely accurate approximation and small coefficients, are mutually exclusive. Thus, stable approximations with propagative plane waves are not possible.

Lemma 4.2. *Let $p \in \mathbb{Z}$ and some tolerance $1 \geq \eta > 0$ be given. The sequence of approximation sets $\{\Phi_M\}_{M \in \mathbb{N}}$ of propagative plane waves with equispaced angles as defined in (4.3) is such that*

$$\forall M \in \mathbb{N}, \boldsymbol{\mu} \in \mathbb{C}^M, \quad \|b_p - \mathcal{T}_{\Phi_M} \boldsymbol{\mu}\|_{\mathcal{B}} \leq \eta \|b_p\|_{\mathcal{B}} \quad \Rightarrow \quad \|\boldsymbol{\mu}\|_{\ell^1} \geq (1 - \eta) \beta_p \|b_p\|_{\mathcal{B}}. \quad (4.8)$$

Proof. Let $M \in \mathbb{N}$ and $\boldsymbol{\mu} := \{\mu_m\}_{m=1}^M \in \mathbb{C}^M$. Using the Jacobi–Anger identity (4.4) we obtain at $\mathbf{x} = (r, \theta) \in B_1$

$$\begin{aligned} (\mathcal{T}_{\Phi_M} \boldsymbol{\mu})(r, \theta) &= \sum_{m=1}^M \mu_m \sum_{q \in \mathbb{Z}} i^q J_q(\kappa r) e^{iq(\theta - \varphi_m)} \\ &= \sum_{q \in \mathbb{Z}} \left(i^q \sum_{m=1}^M \mu_m e^{-iq\varphi_m} \right) J_q(\kappa r) e^{iq\theta} = \sum_{q \in \mathbb{Z}} c_q \tilde{b}_p(r, \theta), \end{aligned} \quad (4.9)$$

where the coefficients $c_q := i^q \sum_{m=1}^M \mu_m e^{-iq\varphi_m}$ satisfy

$$|c_q| = \left| i^q \sum_{m=1}^M \mu_m e^{-iq\varphi_m} \right| \leq \sum_{m=1}^M |\mu_m| = \|\boldsymbol{\mu}\|_{\ell^1} \quad \forall q \in \mathbb{Z}. \quad (4.10)$$

The approximation error is

$$\|b_p - \mathcal{T}_{\Phi_M} \boldsymbol{\mu}\|_{\mathcal{B}}^2 = \sum_{q \in \mathbb{Z}} |\delta_{pq} - c_q \beta_q^{-1}|^2. \quad (4.11)$$

To get the error $\|b_p - \mathcal{T}_{\Phi_M} \boldsymbol{\mu}\|_{\mathcal{B}}$ below the tolerance $\eta > 0$, we need at least

$$|\delta_{pq} - c_q \beta_q^{-1}| < \eta, \quad \forall q \in \mathbb{Z}. \quad (4.12)$$

For $q = p$ this reads

$$\eta > |1 - c_p \beta_p^{-1}| \geq 1 - |c_p| \beta_p^{-1} \geq 1 - \|\boldsymbol{\mu}\|_{\ell^1} \beta_p^{-1}, \quad (4.13)$$

which can be rewritten as (4.8), recalling that $\|b_p\|_{\mathcal{B}} = 1$. \square

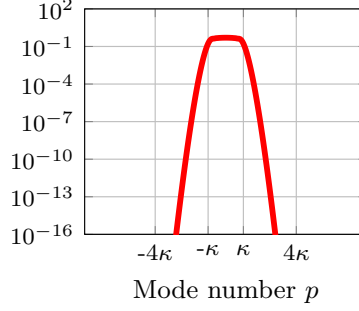


Figure 2: Modal analysis of a propagative plane wave: absolute values of the coefficients of the expansion of ϕ_φ in the basis $\{b_p\}_{p \in \mathbb{Z}}$. Wavenumber $\kappa = 16$.

This bound means that if we approximate circular waves b_p in the form of propagative plane wave expansions $\mathcal{T}_{\Phi_M} \mu$ with a given accuracy (i.e. small $\eta > 0$), then the norms of the coefficients $\|\mu\|_{\ell^1}$ need to increase at least like the normalization constant β_p , i.e. super-exponentially fast in $|p|$, see Lemma 2.4. This is a clear example of how accuracy and stability properties are sometimes opposite to each other. We state this important conclusion in the form of a theorem to stress the message.

Theorem 4.3. *The sequence of approximation sets $\{\Phi_M\}_{M \in \mathbb{N}}$ consisting of propagative plane waves with equispaced angles as defined in (4.3) is not a stable approximation for \mathcal{B} .*

Proof. Lemma 4.2 exhibits a particular sequence, namely the sequence of circular waves $\{b_p\}_{p \in \mathbb{Z}}$, for which the sequence $\{\Phi_M\}_{M \in \mathbb{N}}$ does not provide stable approximations. Indeed, let $p \in \mathbb{Z}$ and suppose that there exists $M \in \mathbb{N}$ and $\mu \in \mathbb{C}^M$ such that $\|b_p - \mathcal{T}_{\Phi_M} \mu\|_{\mathcal{B}} \leq \eta \|b_p\|_{\mathcal{B}}$ for some $0 < \eta < 1$. Then $\|\mu\|_{\ell^1} \geq (1 - \eta) \beta_p \|b_p\|_{\mathcal{B}}$, which implies that $\|\mu\|_{\ell^1}$ can not be bounded uniformly with respect to p in virtue of Lemma 2.4. The stability condition (3.3) is not satisfied for the ℓ^1 norm, hence also for the ℓ^2 norm thanks to (3.4). We conclude that the sequence of approximation sets $\{\Phi_M\}_{M \in \mathbb{N}}$ is unstable in the sense of Definition 3.1. \square

More generally, this statement has implications for other Trefftz methods as well. It is not sufficient to study only the best approximation error in an approximation space spanned by Trefftz elements. If one is interested in numerical methods, one has to study approximation properties in relation to coefficient norm, and the latter depends not only on the approximation space but also on its chosen representation, i.e. the approximation set.

Modal analysis of a propagative plane wave. Another point of view on the same issue is directly given by the Jacobi–Anger identity (4.4). This identity allows us to get quantitative insight into the modal content of propagative plane waves. For any $\mathbf{x} = (r, \theta) \in B_1$ and $\varphi \in [0, 2\pi)$, we have

$$e^{i\kappa \mathbf{d}(\varphi) \cdot \mathbf{x}} = \sum_{p \in \mathbb{Z}} (i^p e^{-ip\varphi} J_p(\kappa r)) e^{ip\theta} = \sum_{p \in \mathbb{Z}} (i^p e^{-ip\varphi} \beta_p^{-1}) b_p(r, \theta). \quad (4.14)$$

The modulus of the coefficients $i^p e^{-ip\varphi} \beta_p^{-1}$ in the expansion as a function of p can be directly deduced from Lemma 2.4 (for large $|p|$) and is reported in Figure 2. This quantity does not depend on the propagation angle φ which parametrizes the propagative plane wave.

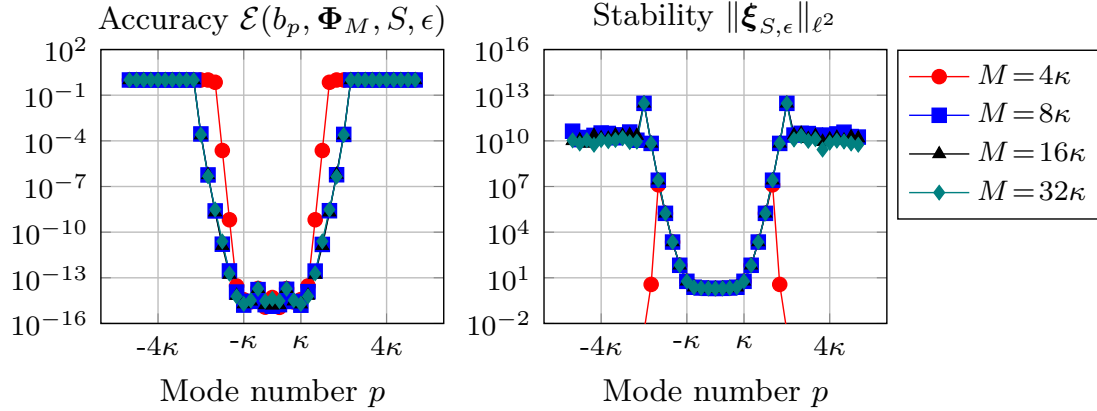


Figure 3: Accuracy \mathcal{E} , as defined in (3.22) (left) and stability $\|\xi_{S,\epsilon}\|_{\ell^2}$ (right) of the approximation of circular waves b_p by propagative plane waves. Wavenumber $\kappa = 16$ and regularization parameter $\epsilon = 10^{-14}$.

These coefficients decay super-exponentially fast in modulus in the evanescent regime $|p| \geq \kappa$. Recalling Remark 2.5, the coefficients with respect to a normalization in alternative sensible norms ($L^2(B_1)$, $L^2(\partial B_1)$ or $L^\infty(\partial B_1)$ for instance) modify the decay only by some moderate powers of $|p|$. This does not come as a surprise, since the propagative plane wave are entire functions. Yet, the modal content of any propagative plane wave is fixed and low-frequency. The direct implication is that they are not suited for approximating Helmholtz solutions with a high-frequency modal content (large $|p|$), as already shown in Lemma 4.2.

4.4 Numerical illustration

The instability result of Lemma 4.2 can easily be verified numerically. Let us consider again the approximation problem of Section 4.3, namely the approximation of the circular wave b_p for some $p \in \mathbb{Z}$ by an approximation set Φ_M of $M \in \mathbb{N}$ propagative plane waves defined in (4.3). The sampling matrix A was defined in (3.7), using M propagative plane waves with equispaced angles and $S := \max(2M, 2|p|)$ sampling points (we impose $S \geq 2|p|$ to avoid spurious results due to aliasing). The entries of the matrix A are immediately computed as $A_{s,m} = e^{i\kappa \cos(2\pi(\frac{s}{S} - \frac{m}{M}))}$ for $s = 1, \dots, S$, $m = 1, \dots, M$. The right-hand side \mathbf{b} is defined as in (3.7) for b_p in place of u ; we recall that we use Dirichlet data in all our numerical experiments.

The matrix A is notoriously ill-conditioned (see Figure 4): its condition number grows exponentially with respect to the number of plane waves M in the approximation set Φ_M . This is a well-known fact, see for instance the numerical experiments in [29, Sec. 2.3] for the circular geometry for the case $S = M$. This is not a feature of the sampling method, and we refer to similar experiments in [20, Sec. 4.3] for the mass matrix of a Galerkin formulation in a Cartesian geometry, again for the case $S = M$. We also point out that the least-squares formulation suffers from an even worse condition number: proportional to the square of the condition number of the sampling method, see e.g. [29, Eq. (30)]. We apply the regularization procedure described in Section 3.3 with threshold parameter $\epsilon = 10^{-14}$.

The numerical results are reported in Figure 3. On the left panel we report the relative residual \mathcal{E} defined in (3.22) as a measure of the accuracy of the approximation. On the right panel we report the size of the coefficients, namely $\|\xi_{S,\epsilon}\|_{\ell^2}$ as a measure of the stability of the

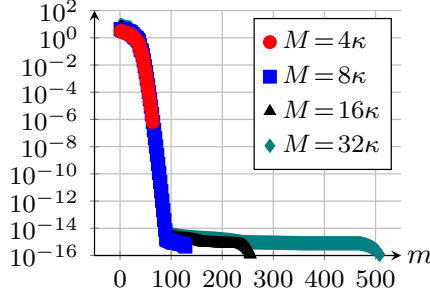


Figure 4: Singular values $\{\sigma_m\}_{m=1}^M$ of the matrix A when using a set of M propagative plane waves. Wavenumber $\kappa = 16$.

approximation. Relative residuals and coefficient norms were already used in [22] to assess the stability of the approximations.

We observe three regimes:

- For the propagative modes, i.e. those corresponding to circular wave with mode number $|p| \leq \kappa$, the approximation is accurate ($\mathcal{E} < 10^{-13}$) and the size of the coefficients is moderate ($\|\xi_{S,\epsilon}\| < 10$).
- For mode numbers $|p|$ roughly larger than the wavenumber κ , the norms of the coefficients of the computed approximations blow up exponentially. The accuracy is spoiled proportionally.
- At some point (roughly between $|p| = 2\kappa$ and $|p| = 3\kappa$ for this particular numerical experiment), the exponential growth of the coefficients completely destroys the stability of the approximation, and we cannot approximate the target b_p with any decent accuracy. Of course, when the relative error is $\mathcal{O}(1)$ the size of the coefficients reported is not meaningful. In fact taking $\xi_{S,\epsilon}$ identically zero would provide a similar error.

Increasing the number of plane waves M has no effect on the accuracy beyond a certain point. Indeed, Figure 4 shows that the ϵ -rank (i.e. the number of singular values larger than ϵ) of the matrix A does not increase when M is raised. Decreasing the regularization parameter ϵ further would not make any significant difference since we use double precision in floating point arithmetic.

Although increasing M does not bring any higher accuracy, it does not increase any further the numerical instability. This is despite the blow up with respect to M of the condition number (ratio of the largest singular value σ_{\max} over the smallest one σ_{\min}) of the matrix A , see Figure 4. For a fixed M , the same matrix A is used to approximate all the b_p 's for any mode number p (i.e. to compute all markers of the same color in Figure 3). Even when the matrix A is extremely ill-conditioned (say $M = 32\kappa$ in the numerical experiments presented here), we get at the same time almost machine-precision accuracy for all propagative modes $|p| \leq \kappa$ while having $\mathcal{O}(1)$ error for evanescent modes with larger mode number $|p| \geq 3\kappa$. It is the simple regularization procedure described in Section 3.3 that allows us to obtain such results.

Any regularization procedure might mitigate but can not overcome the inherent instability of Trefftz methods based on propagative plane waves. In particular, even with regularization, accuracy in the approximation of the evanescent modes remains out of reach for a given floating-point precision. The main objective of this paper is precisely to construct a discrete space of

plane waves that allow the stable approximation of all modes, in view of their use in Trefftz schemes.

5 Evanescent plane waves

The purpose of this section is to introduce evanescent plane waves with defining direction vector $\mathbf{d} \in \mathbb{C}^2$ instead of propagative ones $\mathbf{d} \in \mathbb{R}^2$ and give some intuition on why we expect such waves to have better stability properties.

5.1 Definition

We first provide the definition of an *evanescent plane wave*.

Definition 5.1 (Evanescent plane wave). *For any $\mathbf{y} := (\varphi, \zeta) \in [0, 2\pi) \times \mathbb{R}$, we let*

$$\phi_{\mathbf{y}}(\mathbf{x}) = \phi_{\varphi, \zeta}(\mathbf{x}) := e^{\imath \kappa \mathbf{d}(\mathbf{y}) \cdot \mathbf{x}}, \quad \forall \mathbf{x} \in \mathbb{R}^2, \quad (5.1)$$

where the complex direction of the wave is given by

$$\mathbf{d}(\mathbf{y}) := (\cos(\varphi + \imath \zeta), \sin(\varphi + \imath \zeta)) \in \mathbb{C}^2. \quad (5.2)$$

It is readily checked that the evanescent plane waves are solutions of the homogeneous Helmholtz equation (1.1) since $\mathbf{d}(\mathbf{y}) \cdot \mathbf{d}(\mathbf{y}) = 1$ for any $\mathbf{y} \in [0, 2\pi) \times \mathbb{R}$.

The evanescent plane wave can be seen as propagative plane waves after the ‘complexification’ of the angle $\varphi \in \mathbb{R}$ into $\varphi + \imath \zeta \in \mathbb{C}$. For $\mathbf{y} = (\varphi, 0)$ (i.e. setting $\zeta = 0$), we recover the usual propagative plane wave of Definition 4.1, whose direction is defined solely by the angle φ : $\phi_{\varphi, 0} = \phi_{\varphi}$.

Since the angle is complex, the behavior of the “wave” might be unclear. A more explicit expression of the evanescent plane wave is

$$\phi_{\varphi, \zeta}(\mathbf{x}) = e^{\imath \kappa (\cosh \zeta) \mathbf{x} \cdot \mathbf{d}(\varphi)} e^{-\kappa (\sinh \zeta) \mathbf{x} \cdot \mathbf{d}^{\perp}(\varphi)}, \quad \text{where} \quad \mathbf{d}^{\perp}(\varphi) := (-\sin \varphi, \cos \varphi). \quad (5.3)$$

We see from this formula that the wave *oscillates* with apparent wavenumber $\kappa \cosh \zeta \geq \kappa$ in the direction of $\mathbf{d}(\varphi) := (\cos \varphi, \sin \varphi)$, which was defined in (4.2) and is parallel to $\Re[\mathbf{d}(\mathbf{y})]$. In addition, the wave *decays* exponentially with rate $\kappa \sinh \zeta$ in the (orthogonal) direction $\mathbf{d}(\varphi)^{\perp}$, which is parallel to $\Im[\mathbf{d}(\mathbf{y})]$. This justifies naming the new parameter $\zeta \in \mathbb{R}$, which controls the imaginary part of the angle, the *evanescence* parameter.

In cylindrical coordinates, so adapted to the unit disk, the evanescent plane wave reads

$$\phi_{\varphi, \zeta}(\mathbf{x}) = e^{\imath \kappa r \cosh \zeta \cos(\varphi - \theta)} e^{\kappa r \sinh \zeta \sin(\varphi - \theta)}, \quad \forall \mathbf{x} = (r, \theta) \in \mathbb{R}^2. \quad (5.4)$$

A representation of several evanescent plane waves is given in Figure 5.

5.2 Modal analysis of evanescent plane waves

The Jacobi–Anger expansion (4.4) extends to complex \mathbf{d} , i.e. to evanescent plane waves, see [15, Eq. (10.12.1), (10.11.1)]: for any $\mathbf{x} = (r, \theta) \in B_1$ and $\mathbf{y} = (\varphi, \zeta) \in [0, 2\pi) \times \mathbb{R}$,

$$e^{\imath \kappa \mathbf{d}(\mathbf{y}) \cdot \mathbf{x}} = \sum_{p \in \mathbb{Z}} \imath^p J_p(\kappa r) e^{\imath p(\theta - [\varphi + \imath \zeta])} = \sum_{p \in \mathbb{Z}} (\imath^p e^{-\imath p \varphi} e^{p \zeta} \beta_p^{-1}) b_p(r, \theta). \quad (5.5)$$

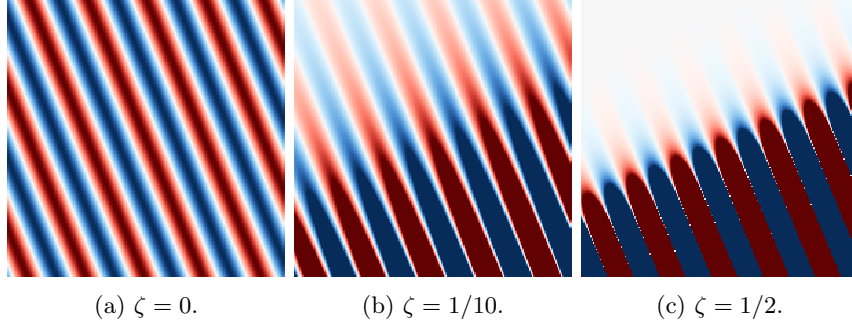


Figure 5: Real part of evanescent plane waves $\phi_{\varphi,\zeta}$ with angle $\varphi = \pi/8$ and wavenumber $\kappa = 16$.

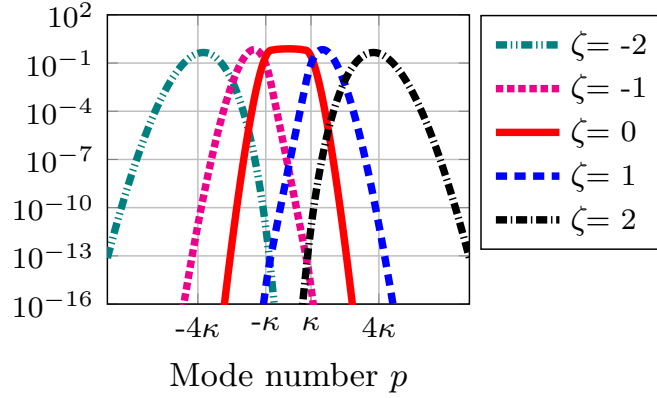


Figure 6: Modal analysis of 5 evanescent plane waves for various evanescence parameter ζ : absolute values of the coefficients of the expansion of $\phi_{\varphi,\zeta}$ in the basis $\{b_p\}_{p \in \mathbb{Z}}$. Wavenumber $\kappa = 16$.

The modulus of the coefficients $v^p e^{-ip\varphi} e^{p\zeta} \beta_p^{-1}$ in the modal expansion are reported in Figure 6 as functions of p . On this graph, we have conveniently normalized the coefficients according to a normalization factor (depending only on ζ) which is described in the following sections, see (7.17).

In comparison with Figure 2, we see that by tuning the evanescence parameter ζ we are able to shift the modal content of the plane waves to higher-frequency regimes. As a result, we expect the evanescent plane waves to be able to capture well the higher-frequency modes of Helmholtz solutions that are less regular (for instance in presence of close-by singularities). The difficulty then is to properly choose suitable values for this new evanescence parameter ζ in order to build approximation spaces that are reasonable in size. This will be the main objective of the remainder of this paper.

6 Mapping Herglotz densities to Helmholtz solutions

In this section we introduce an integral transform between a space of functions defined on the parametric domain $[0, 2\pi) \times \mathbb{R}$ and the space of Helmholtz solutions in the unit disk \mathcal{B} .

6.1 Space of Herglotz densities

To shorten notations we denote in the following the parametric domain as the cylinder

$$Y := [0, 2\pi) \times \mathbb{R}. \quad (6.1)$$

We introduce a weighted L^2 space defined on the cylinder Y . The weight function is (the square of)

$$w_z(\mathbf{y}) = w_z(\zeta) := e^{-\kappa \sinh |\zeta| + z|\zeta|}, \quad \forall \mathbf{y} = (\varphi, \zeta) \in Y, \quad (6.2)$$

and for some $z \in \mathbb{R}$. In this section, the parameter z is temporarily not specified, although the following analysis shows that it cannot be chosen freely and should take the specific value $z = 1/4$, see (6.15). We stress that w_z does not depend on the angle φ . The weighted scalar product and associated norm are then defined by:

$$\begin{aligned} (u, v)_{\mathcal{A}} &:= \int_Y u(\mathbf{y}) \overline{v(\mathbf{y})} w_z^2(\mathbf{y}) d\mathbf{y}, \\ \|u\|_{\mathcal{A}}^2 &:= (u, u)_{\mathcal{A}}. \end{aligned} \quad (6.3)$$

We now introduce a subspace of $L^2(Y; w_z^2)$ which we call space of *Herglotz densities* for reasons that will be clear in the following.

Definition 6.1 (Herglotz polynomials). *We define, for any $p \in \mathbb{Z}$,*

$$\begin{aligned} \tilde{a}_p(\mathbf{y}) &:= e^{p\zeta} e^{ip\varphi}, \quad \forall \mathbf{y} = (\varphi, \zeta) \in Y, \\ a_p &:= \alpha_p \tilde{a}_p, \quad \text{where} \quad \alpha_p := \|\tilde{a}_p\|_{\mathcal{A}}^{-1}, \end{aligned} \quad (6.4)$$

and

$$\mathcal{A} := \overline{\text{span}\{a_p\}_{p \in \mathbb{Z}}}^{\|\cdot\|_{\mathcal{A}}} \subsetneq L^2(Y; w_z^2). \quad (6.5)$$

The wavenumber κ appears explicitly in the weight function w_z . Therefore, each a_p for $p \in \mathbb{Z}$ has an implicit dependence in the wavenumber κ through the normalization factor α_p .

For any $p \in \mathbb{Z}$, the complex-valued function $(\zeta + i\varphi) \mapsto a_p(\varphi, \zeta)$ is a holomorphic function of the complex variable $\zeta + i\varphi \in \mathbb{C}$ for any $(\varphi, \zeta) \in Y$. It follows that its real and imaginary parts are harmonic functions on the cylinder Y .

Lemma 6.2. *The space $(\mathcal{A}, \|\cdot\|_{\mathcal{A}})$ is a Hilbert space and the family $\{a_p\}_{p \in \mathbb{Z}}$ is a Hilbert basis:*

$$(a_p, a_q)_{\mathcal{A}} = \delta_{pq}, \quad \forall p, q \in \mathbb{Z}, \quad \text{and} \quad v = \sum_{p \in \mathbb{Z}} (v, a_p)_{\mathcal{A}} a_p, \quad \forall v \in \mathcal{A}. \quad (6.6)$$

The coefficients α_p decay super-exponentially with $|p|$ after a pre-asymptotic regime up to $|p| \approx \kappa$. The precise asymptotic behavior is given by the following lemma.

Lemma 6.3. *We have*

$$\alpha_p \sim c(\kappa) \left(\frac{e\kappa}{2} \right)^{|p|} |p|^{1/4 - z - |p|} \quad \text{as } |p| \rightarrow +\infty, \quad (6.7)$$

where the constant $c(\kappa)$ only depends on κ .

Proof. It is clear that $\alpha_{-p} = \alpha_p$ for all $p \in \mathbb{Z}$. Let $p \in \mathbb{N}$, we have

$$\begin{aligned}
2\pi \int_{-\infty}^{+\infty} e^{2p\zeta+2z|\zeta|} e^{-2\kappa \sinh|\zeta|} d\zeta &= \|\tilde{a}_p\|_{\mathcal{A}}^2 \leq 2\pi \int_{-\infty}^{+\infty} e^{2p|\zeta|+2z|\zeta|} e^{-2\kappa \sinh|\zeta|} d\zeta, \\
2\pi \int_0^{+\infty} e^{2(p+z)\zeta} e^{-2\kappa \sinh \zeta} d\zeta &\leq \|\tilde{a}_p\|_{\mathcal{A}}^2 \leq 4\pi \int_0^{+\infty} e^{2(p+z)\zeta} e^{-2\kappa \sinh \zeta} d\zeta, \\
2\pi \kappa^{-m} \int_{\kappa}^{+\infty} \eta^{m-1} e^{-\eta+\frac{\kappa^2}{\eta}} d\eta &\leq \|\tilde{a}_p\|_{\mathcal{A}}^2 \leq 4\pi \kappa^{-m} \int_{\kappa}^{+\infty} \eta^{m-1} e^{-\eta+\frac{\kappa^2}{\eta}} d\eta, \\
2\pi \kappa^{-m} \int_{\kappa}^{+\infty} \eta^{m-1} e^{-\eta} d\eta &\leq \|\tilde{a}_p\|_{\mathcal{A}}^2 \leq 4\pi e^{\kappa} \kappa^{-m} \int_{\kappa}^{+\infty} \eta^{m-1} e^{-\eta} d\eta, \\
2\pi \kappa^{-m} \Gamma(m, \kappa) &\leq \|\tilde{a}_p\|_{\mathcal{A}}^2 \leq 4\pi e^{\kappa} \kappa^{-m} \Gamma(m, \kappa),
\end{aligned} \tag{6.8}$$

where we used the change of variable $\eta = \kappa e^{\zeta}$, introduced $m = 2(p+z)$ and used the upper incomplete Gamma function defined in [15, Eq. (8.2.2)]. The Gamma function $\Gamma(m)$ and the upper incomplete counterpart $\Gamma(m, \kappa)$ have the same asymptotic behavior for a fixed κ when m goes to infinity, see [15, Eq. (8.11.5)] which gives the asymptotic behavior of $1 - \Gamma(m, \kappa)/\Gamma(m)$. Using [15, Eq. (5.11.3)] we get

$$\Gamma(m, \kappa) \sim \Gamma(m) \sim \sqrt{2\pi} e^{-m} m^{m-1/2}, \quad \text{as } m \rightarrow \infty. \tag{6.9}$$

We obtain, as $p \rightarrow +\infty$,

$$\kappa^{-2(p+z)} \Gamma(2(p+z), \kappa) \sim \sqrt{\pi} \left(\frac{2}{e\kappa} \right)^{2(p+z)} p^{2(p+z)-1/2} \left(1 + \frac{z}{p} \right)^{2(p+z)-1/2}, \tag{6.10}$$

and the last term is in fact equivalent to e^{2z} at infinity; the claimed result follows. \square

Using our definitions, the Jacobi–Anger expansion (5.5) takes the simple form

$$\phi_{\mathbf{y}}(\mathbf{x}) = \sum_{p \in \mathbb{Z}} i^p \overline{\tilde{a}_p(\mathbf{y})} \tilde{b}_p(\mathbf{x}) = \sum_{p \in \mathbb{Z}} \tau_p \overline{a_p(\mathbf{y})} b_p(\mathbf{x}), \quad \forall (\mathbf{x}, \mathbf{y}) \in B_1 \times Y, \tag{6.11}$$

where we introduced

$$\tau_p := i^p (\alpha_p \beta_p)^{-1}, \quad \forall p \in \mathbb{Z}. \tag{6.12}$$

Formula (6.11) relates the basis $\{a_p\}_{p \in \mathbb{Z}}$ of the space \mathcal{A} to evanescent plane waves $\phi_{\mathbf{y}}$ and circular waves b_p on B_1 and is the key reason for introducing the space \mathcal{A} . The behavior of $|\tau_p|$ is of crucial importance in the following analysis. From the asymptotics given in Lemma 2.4 and Lemma 6.3 we deduce the following result.

Lemma 6.4. *We have*

$$|\tau_p| \sim c(\kappa) |p|^{z-1/4} \quad \text{as } |p| \rightarrow +\infty, \tag{6.13}$$

where the constant $c(\kappa)$ only depends on κ . Hence, choosing $z = 1/4$, we get

$$\tau_- := \inf_{p \in \mathbb{Z}} |\tau_p| > 0, \quad \text{and} \quad \tau_+ := \sup_{p \in \mathbb{Z}} |\tau_p| < \infty. \tag{6.14}$$

It is clear that the uniform bounds for $|\tau_p|$ are possible only for a precise pair of norms for the space of Helmholtz solutions and the space of Herglotz densities. The bounds τ_{\pm} depend implicitly on the wavenumber κ .

The uniform boundedness of τ_p is the key to the following analysis. We set $z = 1/4$ in the remainder of the paper and we let

$$w := w_{1/4}. \quad (6.15)$$

We conclude this subsection with a lemma that will be useful in the following.

Lemma 6.5. *For any $\mathbf{x} \in B_1$, $\mathbf{y} \mapsto \overline{\phi_{\mathbf{y}}(\mathbf{x})} \in \mathcal{A}$.*

Proof. Let $\mathbf{x} \in B_1$ and define $v_{\mathbf{x}} : \mathbf{y} \mapsto \overline{\phi_{\mathbf{y}}(\mathbf{x})}$. We have, using the Jacobi–Anger identity (6.11)

$$v_{\mathbf{x}}(\mathbf{y}) = \sum_{p \in \mathbb{Z}} \overline{\tau_p} \overline{b_p(\mathbf{x})} a_p(\mathbf{y}), \quad \forall \mathbf{y} \in Y. \quad (6.16)$$

Since $\{a_p\}_{p \in \mathbb{Z}}$ is a Hilbert basis for \mathcal{A} , if we write $\mathbf{x} = (r, \theta) \in [0, 1) \times [0, 2\pi)$, we get

$$\|v_{\mathbf{x}}\|_{\mathcal{A}}^2 = \sum_{p \in \mathbb{Z}} |\tau_p b_p(\mathbf{x})|^2 \leq \tau_+^2 \sum_{p \in \mathbb{Z}} \beta_p^2 |J_p(\kappa r)|^2. \quad (6.17)$$

Using the estimates (2.15) and (2.18) from the proof of Lemma 2.4, we get

$$\beta_p^2 |J_p(\kappa r)|^2 \sim \frac{\kappa^2 r^{2|p|}}{2\pi |p|}, \quad \text{as } |p| \rightarrow +\infty, \quad (6.18)$$

from which we conclude that $\|v_{\mathbf{x}}\|_{\mathcal{A}} < \infty$. \square

If $\mathbf{x} \in \partial B_1$, so that $r = |\mathbf{x}| = 1$, then $\mathbf{y} \mapsto \overline{\phi_{\mathbf{y}}(\mathbf{x})}$ does not belong to \mathcal{A} , as it is readily seen from the proof of Lemma 6.5.

6.2 Herglotz transform

We introduce an integral operator T that allows to write every Helmholtz solution in \mathcal{B} as a continuous linear combination of evanescent waves weighted by an element of \mathcal{A} . We also describe its adjoint operator T^* , the corresponding frame and Gram operators S and G , and prove some of their properties. The terminology of this section is borrowed from *Frame Theory*, see [9] for a reference on this field.

Synthesis operator. The first and most important definition concerns the transform that maps Herglotz densities to Helmholtz solutions as we prove next.

Definition 6.6. *For any $v \in \mathcal{A}$, we define the Herglotz transform, denoted by T , as the operator*

$$(Tv)(\mathbf{x}) := \int_Y v(\mathbf{y}) \phi_{\mathbf{y}}(\mathbf{x}) w^2(\mathbf{y}) d\mathbf{y}, \quad \forall \mathbf{x} \in B_1. \quad (6.19)$$

This operator is well-defined on \mathcal{A} thanks to Lemma 6.5. In the setting of continuous-frame theory, see e.g. [9, Eq. (5.27)], this operator is called *synthesis* operator.

Theorem 6.7. *The operator T is bounded and invertible on \mathcal{A} :*

$$\begin{aligned} T : \mathcal{A} &\rightarrow \mathcal{B}, \\ v &\mapsto Tv = \sum_{p \in \mathbb{Z}} \tau_p(v, a_p)_{\mathcal{A}} b_p, \end{aligned} \quad (6.20)$$

and

$$\tau_- \|v\|_{\mathcal{A}} \leq \|Tv\|_{\mathcal{B}} \leq \tau_+ \|v\|_{\mathcal{A}}, \quad \forall v \in \mathcal{A}. \quad (6.21)$$

Proof. Using the Jacobi–Anger formula (6.11), for any $v \in \mathcal{A}$ and $\mathbf{x} \in B_1$ we get

$$\begin{aligned} (Tv)(\mathbf{x}) &= \int_Y \phi_{\mathbf{y}}(\mathbf{x}) v(\mathbf{y}) w^2(\mathbf{y}) d\mathbf{y} = \int_Y \left(\sum_{p \in \mathbb{Z}} \tau_p b_p(\mathbf{x}) \overline{a_p(\mathbf{y})} \right) v(\mathbf{y}) w^2(\mathbf{y}) d\mathbf{y} \\ &= \sum_{p \in \mathbb{Z}} \tau_p \int_Y \overline{a_p(\mathbf{y})} v(\mathbf{y}) w^2(\mathbf{y}) d\mathbf{y} b_p(\mathbf{x}) = \sum_{p \in \mathbb{Z}} \tau_p (v, a_p)_{\mathcal{A}} b_p(\mathbf{x}). \end{aligned} \quad (6.22)$$

Hence, from Lemma 6.2

$$\|Tv\|_{\mathcal{B}}^2 = \sum_{p \in \mathbb{Z}} |\tau_p|^2 |(v, a_p)_{\mathcal{A}}|^2, \quad (6.23)$$

and the result follows from Lemma 6.4. \square

It follows that the Herglotz transform T is bounded and invertible between the space of Herglotz densities \mathcal{A} and the space of Helmholtz solutions \mathcal{B} . The inverse operator T^{-1} can also be written as an integral operator: for any $u \in \mathcal{B}$,

$$(T^{-1}u)(\mathbf{y}) = \int_{B_1} u(\mathbf{x}) \Psi(\mathbf{x}, \mathbf{y}) d\mathbf{x} + \kappa^{-2} \int_{B_1} \nabla u(\mathbf{x}) \cdot \nabla \Psi(\mathbf{x}, \mathbf{y}) d\mathbf{x}, \quad \forall \mathbf{y} \in Y, \quad (6.24)$$

where the kernel is defined, for any $\mathbf{y} \in Y$, as

$$\Psi(\mathbf{x}, \mathbf{y}) := \sum_{p \in \mathbb{Z}} \tau_p^{-1} a_p(\mathbf{y}) \overline{b_p(\mathbf{x})}. \quad \forall \mathbf{x} \in B_1. \quad (6.25)$$

Moreover, we have the following direct corollary.

Corollary 6.8. *We have*

$$Ta_p = \tau_p b_p, \quad \forall p \in \mathbb{Z}. \quad (6.26)$$

The integral representation Tv in (6.19) is similar to the Herglotz representation (4.5). This is the reason why we refer to elements of \mathcal{A} as *Herglotz densities*.

As we explained in Section 4.2, not all Helmholtz solutions admit a Herglotz representation that uses only propagative plane waves (4.5) (with density $v \in L^2(\partial B_1)$). In contrast, by allowing evanescent waves, the generalized Herglotz representation (6.19) can represent any Helmholtz solution. Indeed, since T is an isomorphism between \mathcal{A} and \mathcal{B} , for any $u \in \mathcal{B}$, there exists a unique $v \in \mathcal{A}$ such that $u = Tv$. The price to pay for this result is the need for a two-dimensional parameter domain (the cylinder Y) in place of a one-dimensional one (∂B_1) and thus of a double integral; the added dimension corresponds to the evanescence parameter ζ .

In some sense, Theorem 6.7 is a stability result stated at the continuous level. What we aim next is to obtain a discrete version of this integral representation.

Analysis operator. In the continuous-frame setting, see [9, Eq. (5.28)], the adjoint operator T^* of T is called *analysis* operator.

Lemma 6.9. *The adjoint T^* of T is given for any $u \in \mathcal{B}$ by*

$$(T^*u)(\mathbf{y}) := (u, \phi_{\mathbf{y}})_{\mathcal{B}}, \quad \forall \mathbf{y} \in Y. \quad (6.27)$$

The operator T^ is bounded and invertible on \mathcal{B} :*

$$\begin{aligned} T^* &: \mathcal{B} \rightarrow \mathcal{A}, \\ u &\mapsto T^*u = \sum_{p \in \mathbb{Z}} \overline{\tau_p} (u, b_p)_{\mathcal{B}} a_p, \end{aligned} \quad (6.28)$$

and

$$\tau_- \|u\|_{\mathcal{B}} \leq \|T^*u\|_{\mathcal{A}} \leq \tau_+ \|u\|_{\mathcal{B}}, \quad \forall u \in \mathcal{B}. \quad (6.29)$$

Proof. We have, for any $v \in \mathcal{A}$ and $u \in \mathcal{B}$

$$\begin{aligned} (Tv, u)_{\mathcal{B}} &= \left(\int_Y \phi_{\mathbf{y}} v(\mathbf{y}) w^2(\mathbf{y}) d\mathbf{y}, u \right)_{\mathcal{B}} = \int_Y v(\mathbf{y}) (\phi_{\mathbf{y}}, u)_{\mathcal{B}} w^2(\mathbf{y}) d\mathbf{y} \\ &= \left(v, \overline{(\phi_{\mathbf{y}}, u)_{\mathcal{B}}} \right)_{\mathcal{A}} = (v, (u, \phi_{\mathbf{y}})_{\mathcal{B}})_{\mathcal{A}}. \end{aligned} \quad (6.30)$$

In addition, using the Jacobi–Anger formula (6.11), for any $u \in \mathcal{B}$ and $\mathbf{y} \in Y$

$$(T^*u)(\mathbf{y}) = (u, \phi_{\mathbf{y}})_{\mathcal{B}} = \left(u, \sum_{p \in \mathbb{Z}} \tau_p \overline{a_p(\mathbf{y})} b_p \right)_{\mathcal{B}} = \sum_{p \in \mathbb{Z}} \overline{\tau_p} (u, b_p)_{\mathcal{B}} a_p(\mathbf{y}). \quad (6.31)$$

Hence, from Lemma 2.2

$$\|T^*u\|_{\mathcal{A}}^2 = \sum_{p \in \mathbb{Z}} |\tau_p|^2 |(u, b_p)_{\mathcal{B}}|^2, \quad (6.32)$$

and the result follows from Lemma 6.4. \square

Frame and Gram operators. Using the continuous frame terminology, we introduce respectively the *frame operator* and *Gram operator*

$$\begin{aligned} S &:= TT^* : \mathcal{B} \rightarrow \mathcal{B}, \\ G &:= T^*T : \mathcal{A} \rightarrow \mathcal{A}. \end{aligned} \quad (6.33)$$

The frame operator admits the more explicit formula: for any $u \in \mathcal{B}$,

$$Su(\mathbf{x}) = \int_Y (u, \phi_{\mathbf{y}})_{\mathcal{B}} \phi_{\mathbf{y}}(\mathbf{x}) w^2(\mathbf{y}) d\mathbf{y}, \quad \forall \mathbf{x} \in B_1. \quad (6.34)$$

Corollary 6.10. *The operators S and G are bounded, invertible, self-adjoint and positive operators. For any $v \in \mathcal{A}$ and $u \in \mathcal{B}$*

$$\begin{aligned} Su &= \sum_{p \in \mathbb{Z}} |\tau_p|^2 (u, b_p)_{\mathcal{B}} b_p, \\ Gv &= \sum_{p \in \mathbb{Z}} |\tau_p|^2 (v, a_p)_{\mathcal{A}} a_p, \end{aligned} \quad \text{and} \quad \begin{aligned} \tau_-^2 \|u\|_{\mathcal{B}} &\leq \|Su\|_{\mathcal{B}} \leq \tau_+^2 \|u\|_{\mathcal{B}}, \\ \tau_-^2 \|v\|_{\mathcal{A}} &\leq \|Gv\|_{\mathcal{A}} \leq \tau_+^2 \|v\|_{\mathcal{A}}. \end{aligned} \quad (6.35)$$

Proof. This result stems directly from Theorem 6.7 and Lemma 6.9. \square

A continuous frame result. We are now ready to prove that the evanescent plane waves form a continuous frame for the space of Helmholtz solutions in the unit disk.

Theorem 6.11. *The family $\{\phi_{\mathbf{y}}\}_{\mathbf{y} \in Y}$ is a continuous frame for \mathcal{B} . Besides, the optimal frame bounds are $A = \tau_-^2$ and $B = \tau_+^2$.*

Proof. We need to verify the definition of a continuous frame, see [9, Def. 5.6.1]. For any $u \in \mathcal{B}$, the measurability of

$$\mathbf{y} \mapsto (u, \phi_{\mathbf{y}})_{\mathcal{B}} = (T^*u)(\mathbf{y}), \quad (6.36)$$

stems from $T^*u \in \mathcal{A}$ according to Lemma 6.9 and $\mathcal{A} \subset L^2(Y; w^2)$. The frame condition, namely

$$A\|u\|_{\mathcal{B}}^2 \leq \int_Y |(u, \phi_{\mathbf{y}})_{\mathcal{B}}|^2 w^2(\mathbf{y}) d\mathbf{y} \leq B\|u\|_{\mathcal{B}}^2, \quad \forall u \in \mathcal{B}, \quad (6.37)$$

for some constants A and B is a consequence of the boundedness and positivity of the frame operator S which was established in Corollary 6.10. Indeed, for any $u \in \mathcal{B}$, we have

$$\int_Y |(u, \phi_{\mathbf{y}})_{\mathcal{B}}|^2 w^2(\mathbf{y}) d\mathbf{y} = (Su, u)_{\mathcal{B}} = \sum_{p \in \mathbb{Z}} |\tau_p|^2 |(u, b_p)_{\mathcal{B}}|^2, \quad (6.38)$$

which also establishes the optimality of the claimed frame bounds. \square

6.3 The reproducing kernel property

An interesting corollary of the continuous frame result is given by the following proposition. For a general reference on Reproducing Kernel Hilbert Spaces (RKHS), we refer to [28].

Proposition 6.12. *The range \mathcal{A} of the analysis operator T^* has the reproducing kernel property. The reproducing kernel is given by*

$$K(\mathbf{z}, \mathbf{y}) = K_{\mathbf{y}}(\mathbf{z}) = (K_{\mathbf{y}}, K_{\mathbf{z}})_{\mathcal{A}} = \sum_{p \in \mathbb{Z}} \overline{a_p(\mathbf{y})} a_p(\mathbf{z}), \quad \forall \mathbf{y}, \mathbf{z} \in Y, \quad (6.39)$$

with pointwise convergence of the series and where $K_{\mathbf{y}} \in \mathcal{A}$ is the (unique) Riesz representation of the evaluation functional at $\mathbf{y} \in Y$, namely

$$v(\mathbf{y}) = (v, K_{\mathbf{y}})_{\mathcal{A}}, \quad \forall v \in \mathcal{A}. \quad (6.40)$$

Proof. Take any $v \in \mathcal{A}$ and let $u \in \mathcal{B}$ such that $v = T^*u$, which exists thanks to Lemma 6.9. From Corollary 6.10, we have

$$u = S^{-1}Su = \int_Y (u, \phi_{\mathbf{z}})_{\mathcal{B}} S^{-1}\phi_{\mathbf{z}} w^2(\mathbf{z}) d\mathbf{z}. \quad (6.41)$$

Then we obtain the reproducing identity, for any $\mathbf{y} \in Y$

$$\begin{aligned} v(\mathbf{y}) &= (T^*u)(\mathbf{y}) = (u, \phi_{\mathbf{y}})_{\mathcal{B}} = \int_Y (u, \phi_{\mathbf{z}})_{\mathcal{B}} (S^{-1}\phi_{\mathbf{z}}, \phi_{\mathbf{y}})_{\mathcal{B}} w^2(\mathbf{z}) d\mathbf{z} \\ &= \int_Y v(\mathbf{z}) (S^{-1}\phi_{\mathbf{z}}, \phi_{\mathbf{y}})_{\mathcal{B}} w^2(\mathbf{z}) d\mathbf{z} = (v, K_{\mathbf{y}})_{\mathcal{A}}, \end{aligned} \quad (6.42)$$

where we introduced (the Riesz representation of) the evaluation functional at the point \mathbf{y} defined as

$$K_{\mathbf{y}}(\mathbf{z}) := (\phi_{\mathbf{y}}, S^{-1}\phi_{\mathbf{z}})_{\mathcal{B}}, \quad \forall \mathbf{z} \in Y. \quad (6.43)$$

It is a direct consequence of Corollary 6.10 that the kernel admits the series representation (6.39). Alternatively, we refer to [28, Th. 2.4] for a direct proof of this result (valid in the general setting), since $\{a_p\}_{p \in \mathbb{Z}}$ is an orthonormal basis for \mathcal{A} . \square

We emphasize that the reproducing kernel property implies that pointwise evaluation of elements of \mathcal{A} in the cylinder Y is a continuous operation [28, Def. 1.2]. Let $\mathbf{y} \in Y$, then for some $c > 0$ (that may depend on \mathbf{y})

$$|v(\mathbf{y})| = |(v, K_{\mathbf{y}})_{\mathcal{A}}| \leq c\|v\|_{\mathcal{A}}, \quad \forall v \in \mathcal{A}. \quad (6.44)$$

The interest in introducing the reproducing kernel property stems from the following result, which is a direct consequence of Proposition 6.12, Corollary 6.8 and the Jacobi–Anger identity (6.11).

Corollary 6.13. *The evanescent plane waves are the images under T of the Riesz representation of the evaluation functionals, namely*

$$\phi_{\mathbf{y}} = TK_{\mathbf{y}}, \quad \forall \mathbf{y} \in Y. \quad (6.45)$$

As a consequence, the construction of an approximation of a Helmholtz solution $u \in \mathcal{B}$ as an expansion of evanescent plane waves is, up to the isomorphism T , equivalent to the approximation of its Herglotz density $v := T^{-1}u \in \mathcal{A}$ as an expansion of evaluation functionals, i.e.

$$v \approx \sum_{m=1}^M \mu_m K_{\mathbf{y}_m} \quad \xleftrightarrow[T^{-1}]{T} \quad u \approx \sum_{m=1}^M \mu_m \phi_{\mathbf{y}_m}, \quad (6.46)$$

for some set of coefficients $\boldsymbol{\mu} = \{\mu_m\}_{m=1}^M$. The next sections provide numerical evidence that we can indeed build such suitable approximations (up to some normalization of the families $\{K_{\mathbf{y}_m}\}_m$ and $\{\phi_{\mathbf{y}_m}\}_m$).

7 A concrete evanescent plane wave approximation set

We describe below a method for the numerical approximation of a general Helmholtz solution in the unit disk by evanescent plane waves.

We exploit the equivalence of this approximation problem with the approximation problem of the corresponding Herglotz density, see (6.46). The main idea is to adapt the sampling procedure of [19, 10] (sometimes called *coherence-optimal sampling*) to our case, in order to generate a distribution of sampling nodes in the cylinder Y that will be used to reconstruct the Herglotz density. Despite having an unbounded parametric domain Y , the finite integrability of the weight function w^2 allows to sampling Y on a bounded region only.

Let $u \in \mathcal{B}$ be the Helmholtz solution, target of the approximation problem, and let $v := T^{-1}u \in \mathcal{A}$ be its associated Herglotz density. Let also some tolerance $\eta > 0$ be given.

7.1 Truncation of the modal expansion

Although u (resp. v) *a priori* lives in an infinite dimensional space \mathcal{B} (resp. \mathcal{A}), the idea is to exploit the natural hierarchy of finite dimensional subspaces constructed by truncation of the Hilbert basis.

Truncation in the Helmholtz solution space. For any $P \in \mathbb{N}$, we define

$$\mathcal{B}_P := \text{span} \{b_p\}_{|p| \leq P} \subset \mathcal{B}. \quad (7.1)$$

We also introduce the orthogonal projection Π_P onto \mathcal{B}_P defined as

$$\begin{aligned} \Pi_P : \mathcal{B} &\rightarrow \mathcal{B}, \\ u &\mapsto \sum_{|p| \leq P} (u, b_p)_{\mathcal{B}} b_p. \end{aligned} \quad (7.2)$$

A natural approach is to try to approximate the projection of u onto \mathcal{B}_P , namely

$$u_P := \Pi_P u \in \mathcal{B}_P, \quad \forall P \in \mathbb{N}, \quad (7.3)$$

for some P large enough. It is immediate that the sequence of projections $\{u_P\}_{P \in \mathbb{N}}$ converges to u in \mathcal{B} . In particular, we can define for any $\eta > 0$

$$P^* = P^*(u, \eta) := \min \{P \in \mathbb{N} \mid \|u - u_P\|_{\mathcal{B}} < \eta \|u\|_{\mathcal{B}}\}. \quad (7.4)$$

Unfortunately, it is not possible to compute such a P^* in most practical configurations. It may be possible though to give estimates on P^* , based on some regularity assumption on u and the decay of its coefficients in its modal expansion. For instance, it might be physically realistic to assume that all coefficients of the propagative modes $|p| \leq \kappa$ are $\mathcal{O}(1)$ and the coefficients associated to the subsequent evanescent modes $|p| \geq \kappa$ decay in modulus with a given algebraic or exponential rate. Yet, there always exists a regular solution with an $\mathcal{O}(1)$ coefficient corresponding to an arbitrarily large mode number $|p|$.

Truncation in the Herglotz density space. Similarly, for any $P \in \mathbb{N}$, we define

$$\mathcal{A}_P := \text{span} \{a_p\}_{|p| \leq P} \subset \mathcal{A}. \quad (7.5)$$

We denote by

$$v_P := T^{-1}u_P \in \mathcal{A}_P, \quad \forall P \in \mathbb{N}, \quad (7.6)$$

the image under the inverse transform of the projection u_P of u onto \mathcal{B}_P .

Theorem 6.7 implies that the sequence $\{v_P\}_{P \in \mathbb{N}}$ converges to v in \mathcal{A} . In particular, for any $P \geq P^*$, where P^* was defined in (7.4), we have

$$\|v - v_P\|_{\mathcal{A}} \leq \tau_-^{-1} \|u - u_P\|_{\mathcal{B}} < \tau_-^{-1} \eta \|u\|_{\mathcal{B}}. \quad (7.7)$$

7.2 Parameter sampling in the cylinder Y

Our objective will now be to approximate for any $P \in \mathbb{N}$ the image of the truncation $v_P = T^{-1}u_P \in \mathcal{A}_P$ (which will subsequently yield an approximation of u_P). In this subsection let us fix a $P \in \mathbb{N}$, not necessarily equal to P^* .

We propose to build approximations of elements of \mathcal{A}_P by constructing a finite set of sampling nodes $\{\mathbf{y}_m\}_m$ in the cylinder Y according to the distribution advocated in [19, Sec. 2.1] and [10, Sec. 2.2]. The associated set of sampling functionals $\{K_{\mathbf{y}_m}\}_m$ (up to some normalization factor) is expected to provide a good approximation of v_P . The approximation set for u_P will then be given by the evanescent plane waves $\{\phi_{\mathbf{y}_m}\}_m$ (up to some normalization factor).

We denote the dimension of the space \mathcal{A}_P by

$$N = N(P) := \dim \mathcal{B}_P = \dim \mathcal{A}_P = 2P + 1. \quad (7.8)$$

The probability density function ρ_N is defined (up to normalization) as the reciprocal of the N -term *Christoffel function* μ_N in the spirit of [10, Eq. (2.6)]:

$$\rho_N := \frac{w^2}{N\mu_N}, \quad \text{where} \quad \mu_N(\mathbf{y}) := \left(\sum_{|p| \leq P} |a_p(\mathbf{y})|^2 \right)^{-1}, \quad \forall \mathbf{y} = (\zeta, \varphi) \in Y. \quad (7.9)$$

Observe that ρ_N and μ_N are well-defined since $0 < \mu_N \leq \mu_1 < \infty$ from the fact that a_0 is just a non-vanishing constant.

In our setting, the density function ρ_N is a univariate function on Y since it is independent of the angle φ . We point out that $1/\mu_N$ corresponds to the truncated series expansion of the diagonal of the reproducing kernel K , which amounts to take $\mathbf{z} = \mathbf{y}$ and truncate at P the series in (6.39).

Let us assume that we can generate a sequence of sampling node sets

$$\mathbb{Y}_P := \{\mathbb{Y}_{P,M}\}_{M \in \mathbb{N}}, \quad \text{where} \quad \mathbb{Y}_{P,M} := \{\mathbf{y}_{P,M,m}\}_{m=1}^M, \quad \forall M \in \mathbb{N}, \quad (7.10)$$

using one's preferred sampling strategy that converges (in a suitable sense) to the distribution density ρ_N . The sampling method could be a deterministic, a random or even a quasi-random strategy, see Section 8. The sets are not assumed to be nested.

This choice of evanescent plane wave parameters is a major difference from the heuristic [22, Eq. (5)] where the parameters are chosen in order to approximate solutions defined in a rectangle containing the physical domain of interest (B_1 in our case).

Associated to the sampling node sets, we introduce a sequence of finite sets in \mathcal{A}

$$\Psi_P := \{\Psi_{P,M}\}_{M \in \mathbb{N}} \quad \text{where} \quad \Psi_{P,M} := \{\psi_{P,M,m}\}_{m=1}^M, \quad \forall M \in \mathbb{N}, \quad (7.11)$$

and

$$\psi_{P,M,m} := \sqrt{\mu_N(\mathbf{y}_{P,M,m})} K_{\mathbf{y}_{P,M,m}}, \quad 1 \leq m \leq M. \quad (7.12)$$

In the approximation sets, each $K_{\mathbf{y}_{P,M,m}}$ has been normalized by the real constant $\sqrt{\mu_N(\mathbf{y}_{P,M,m})}$ which is (numerically) close to $\|K_{\mathbf{y}_{P,M,m}}\|_{\mathcal{A}}^{-1}$. More precisely, we have

$$\frac{\|K_{\mathbf{y}}\|_{\mathcal{A}}}{\sqrt{\mu_N(\mathbf{y})}} = \left(\sum_{p \in \mathbb{Z}} |a_p(\mathbf{y})|^2 \right)^{1/2} \left(\sum_{|p| \leq P} |a_p(\mathbf{y})|^2 \right)^{-1/2} \geq 1, \quad \forall \mathbf{y} \in Y. \quad (7.13)$$

The normalization (7.12) is crucial for the numerical stability of the scheme. Recall that the stable approximation property (3.3) of a set sequence depends on the normalization of its elements.

We can state now our main conjecture, which is corroborated by the numerical experiments given in the next section.

Conjecture 7.1. *The sequence of approximation sets Ψ_P defined in (7.11) is a stable approximation for \mathcal{A}_P . Namely, there exist $s = s(P) \geq 0$ and $C = C(P) \geq 0$ such that*

$$\forall v_P \in \mathcal{A}_P, \exists M \in \mathbb{N}, \boldsymbol{\mu} \in \mathbb{C}^M, \quad \|v_P - \mathcal{T}_{\Psi_{P,M}} \boldsymbol{\mu}\|_{\mathcal{A}} \leq \eta \|v_P\|_{\mathcal{A}} \quad \text{and} \quad \|\boldsymbol{\mu}\|_{\ell^2} \leq CM^s \|v_P\|_{\mathcal{A}}. \quad (7.14)$$

Moreover, the smallest such stability exponent $s = s(P)$ and the smallest such stability constant $C = C(P)$ are bounded uniformly with respect to the truncation parameter P , namely

$$s^* := \sup_{P \in \mathbb{N}} \{s(P)\} < \infty, \quad C^* := \sup_{P \in \mathbb{N}} \{C(P)\} < \infty. \quad (7.15)$$

Assuming Conjecture 7.1 holds, we can define

$$M^* = M^*(u, P, \eta) := \min \{M \in \mathbb{N} \mid \exists \boldsymbol{\mu} \in \mathbb{C}^M, \|v_P - \mathcal{T}_{\Psi_{P,M}} \boldsymbol{\mu}\|_{\mathcal{A}} < \eta \|v_P\|_{\mathcal{A}} \text{ and } \|\boldsymbol{\mu}\|_{\ell^2} \leq CM^s \|v_P\|_{\mathcal{A}}\}. \quad (7.16)$$

In the following we assume for simplicity that all $M \geq M^*$ satisfy the two inequalities appearing in (7.16) (otherwise the proofs can be easily adapted). This holds true if the sets are hierarchical, for instance, but this is not necessary.

The available analysis in the literature suggests that the number of sampling nodes M^* to achieve accuracy (irrespectively of the stability property which, to the best of our knowledge, is not studied in the literature) should scale log-linearly with the dimension N of the finite dimensional subspace \mathcal{A}_P , that is $M^* = \mathcal{O}(N \log N)$, see [19, Th. 2.1] and [10, Th. 2.1 and Cor. 2.2]. We investigate numerically this question in Section 8.4.

7.3 Stability of evanescent plane wave sets

Associated to the sampling set sequences (7.10) and approximation set sequences (7.11) (in \mathcal{A}), we define the sequence of approximation sets of (normalized) evanescent plane waves in \mathcal{B} as follows

$$\Phi := \{\Phi_{P,M}\}_{P \in \mathbb{N}, M \in \mathbb{N}}, \quad \Phi_{P,M} := \left\{ \sqrt{\frac{\mu_N(\mathbf{y}_{P,M,m})}{M}} \phi_{\mathbf{y}_{P,M,m}} \right\}_{m=1}^M, \quad \forall P \in \mathbb{N}, M \in \mathbb{N}. \quad (7.17)$$

We use a double index (P, M) for each approximation set $\Phi_{P,M}$ because for each $P \in \mathbb{N}$ we generate a sequence of sampling point sets $\Psi_P := \{\Psi_{P,M}\}_{M \in \mathbb{N}}$ (see (7.10)) such that $|\Psi_{P,M}| = M$ for all $M \in \mathbb{N}$ and that converges as M tends to infinity to the density $\rho_{N(P)}$ defined in (7.9).

Proposition 7.2. *Let $\delta > 0$. If Conjecture 7.1 holds then the sequence of approximation sets (7.17) provides a stable approximation for \mathcal{B} . In particular, if κ^2 is not a Dirichlet eigenvalue on B_1 ,*

$$\forall u \in \mathcal{B} \cap C^0(\overline{B_1}), \exists P \in \mathbb{N}, M \in \mathbb{N}, S \in \mathbb{N}, \epsilon \in (0, 1], \quad \|u - \mathcal{T}_{\Phi_{P,M}} \xi_{S,\epsilon}\|_{L^2(B_1)} \leq \delta \|u\|_{\mathcal{B}}, \quad (7.18)$$

where $\xi_{S,\epsilon} \in \mathbb{C}^{|\Phi_{P,M}|}$ is computed with the regularization procedure in (3.10). The SVD regularization parameter ϵ can be chosen as (3.19).

Proof. We need to prove the stability of the sequence of approximation sets, namely that for any $\tilde{\eta} > 0$, there exists $s \geq 0$ and $C \geq 0$ such that

$$\forall u \in \mathcal{B}, \exists P \in \mathbb{N}, M \in \mathbb{N}, \mu \in \mathbb{C}^M, \quad \|u - \mathcal{T}_{\Phi_{P,M}} \mu\|_{\mathcal{B}} \leq \tilde{\eta} \|u\|_{\mathcal{B}} \quad \text{and} \quad \|\mu\|_{\ell^2} \leq CM^s \|u\|_{\mathcal{B}}. \quad (7.19)$$

Provided this holds, the claimed result is a direct application of Corollary 3.3.

Let $\eta > 0$, $u \in \mathcal{B}$ and set $v := T^{-1}u \in \mathcal{A}$. For any $P \geq P^*(u, \eta)$ with P^* defined in (7.4), if we let $u_P := \Pi_P u$ and $v_P := T^{-1}u_P$ we have (recall (7.7))

$$\|u - u_P\|_{\mathcal{B}} \leq \eta \|u\|_{\mathcal{B}}, \quad \text{and} \quad \|v - v_P\|_{\mathcal{A}} \leq \tau_-^{-1} \eta \|u\|_{\mathcal{B}}. \quad (7.20)$$

Assuming that Conjecture 7.1 holds, there exist s^* and C^* (both independent of P) such that, for any $M \geq M^*(u, P, \eta)$ with M^* defined in (7.16), there exists a set of coefficients $\mu \in \mathbb{C}^M$ such that

$$\|v_P - \mathcal{T}_{\Psi_{P,M}} \mu\|_{\mathcal{A}} \leq \eta \|v_P\|_{\mathcal{A}}, \quad \text{and} \quad \|\mu\|_{\ell^2} \leq C^* M^{s^*} \|v_P\|_{\mathcal{A}}. \quad (7.21)$$

The properties of the isomorphism T given in Theorem 6.7 imply that

$$\|u_P - \mathcal{T}_{\Phi_{P,M}} \mu\|_{\mathcal{B}} < \tau_+ \eta \|v_P\|_{\mathcal{A}} \quad \text{and} \quad \|v_P\|_{\mathcal{A}} \leq \tau_-^{-1} \|u_P\|_{\mathcal{B}} \leq \tau_-^{-1} \|u\|_{\mathcal{B}}. \quad (7.22)$$

For any $P \geq P^*(u, \eta)$ and $M \geq M^*(u, P, \eta)$, the total approximation error for the Herglotz density v can be estimated as

$$\|v - \mathcal{T}_{\Phi_{P,M}} \mu\|_{\mathcal{A}} \leq \|v - v_P\|_{\mathcal{A}} + \|v_P - \mathcal{T}_{\Psi_{P,M}} \mu\|_{\mathcal{A}} \leq 2\tau_-^{-1} \eta \|u\|_{\mathcal{B}}, \quad (7.23)$$

and for the Helmholtz solution u as

$$\begin{aligned} \|u - \mathcal{T}_{\Phi_{P,M}} \mu\|_{\mathcal{B}} &\leq \|u - u_P\|_{\mathcal{B}} + \|u_P - \mathcal{T}_{\Phi_{P,M}} \mu\|_{\mathcal{B}} \\ &\leq (1 + \tau_+ \tau_-^{-1}) \eta \|u\|_{\mathcal{B}}, \end{aligned} \quad \text{and} \quad \|\mu\|_{\ell^2} \leq C^* M^{s^*} \tau_-^{-1} \|u\|_{\mathcal{B}}. \quad (7.24)$$

We conclude by choosing $\eta = \tilde{\eta}/(1 + \tau_+ \tau_-^{-1})$ and noting that (7.24) is (7.19) with $s = s^*$ and $C = C^* \tau_-^{-1}$. \square

The uniform boundedness of the stability exponent $s = s(P)$ and the stability constant $C = C(P)$ in Conjecture 7.1 is an essential ingredient of the proof above since $P \geq P^*$ depends on u . Without the uniform boundedness, Conjecture 7.1 would be too weak to establish (7.19).

Discussion on the parameters. In view of practical implementations, the proof of Proposition 7.2 is instructive. Our numerical recipe for building the approximation sets $\Phi_{P,M}$ is based on only two parameters, P and M whose tuning is intuitive:

1. The first one is the Fourier truncation parameter P which controls the first term in the error estimates (7.24) and (7.23). The appropriate value for $P \geq P^*$ will solely depend on the decay of the coefficients in the modal expansion, which is intimately linked to the regularity of the Helmholtz solution.
2. The second one is the dimension M of the evanescent-wave approximation space, which is also the number of sampling points in the parameter cylinder Y . For a fixed P , increasing M allows to control the second term in the error estimates (7.24) and (7.23). The conjecture states that taking a sufficiently large M yields small errors with bounded coefficients. The numerical results presented below show experimentally that M should scale linearly with P , with a moderate proportionality constant (see Section 8.4).

Once the approximation sets are constructed, our concrete implementation (see Section 3.3) to compute a particular set of coefficients $\xi_{S,\epsilon}$ includes two additional parameters:

1. The number S of sampling points on the boundary of the physical domain B_1 . According to (3.13) and following [1, 2], sufficient oversampling should be used. In practice, we chose for simplicity an oversampling ratio of 2, namely $S = 2M$.
2. The regularization parameter ϵ for the truncation of the singular values. In the numerical experiments below, we set this parameter to 10^{-14} .

The fact that our approximation spaces provide stable approximation in \mathcal{B} is not specific to a particular reconstruction and regularization strategy. Although we chose to focus on the simple method of boundary sampling together with regularized SVD, alternative reconstruction strategies (such as sampling in the bulk of the domain or taking inner product with elements of other types of test spaces for instance) and other regularization techniques (such as Tikhonov regularization) can also be successfully used in practice. Irrespective of the strategy, sufficient oversampling and regularization (hence similar types of parameters) need to be used.

8 Numerical results

We provide below some numerical evidence that the procedure described so far allows to compute controllably accurate approximations of Helmholtz solutions in the unit disk¹.

8.1 Probability densities and samples

Probability density and cumulative distributions functions. We represent the probability density functions $\rho_{N(P)}$ (see (7.9)) as functions of the evanescence parameter ζ in the left column of Figure 7. Here P denotes the truncation parameter, meaning that the sampling is performed to approximate elements of \mathcal{A}_P , which has dimension $N(P)$. The associated cumulative distribution functions with respect to the evanescence parameter ζ are defined as

$$\Upsilon_N(\zeta) := \int_{-\infty}^{\zeta} \rho_N(\tilde{\zeta}) \, d\tilde{\zeta}, \quad \forall \zeta \in \mathbb{R}. \quad (8.1)$$

¹The JULIA code used to generate the numerical results of this paper is available at <https://github.com/EmileParolin/evanescent-plane-wave-approx>

They are represented in the right column of Figure 7.

Recall that while ρ_N is a bi-variate function on the cylinder Y , it is constant with respect to the angle φ . As a result, the cumulative distribution with respect to this variable φ is a linear function. This is why we represent these two functions $\rho_{N(P)}$ and $\Upsilon_{N(P)}$ only with respect to the evanescence parameter ζ .

We observe that the probability densities $\rho_{N(P)}$ are symmetric even functions and exhibit a main mode at $\zeta = 0$ which corresponds to purely propagative plane waves. Moreover, the ϵ -support of these densities is rather tight and the probability eventually tends to zero exponentially as $|\zeta|$ gets large enough. The main mode is higher (i.e. parameters with a small ζ are more likely to be sampled) when the wavenumber is larger. When $P \leq \kappa$ the densities are unimodal distributions whereas for $P \gg \kappa$ (e.g. $P = 4\kappa$) the densities are multimodal distributions. Indeed, in the latter case, there are two symmetric modes for relatively large evanescence parameter, in addition to the main mode at $\zeta = 0$.

The cumulative distribution functions $\Upsilon_{N(P)}$ are close to a step function in the case where \mathcal{A}_P contains only elements associated to the propagative regime $P \leq \kappa$. This is especially true if the wavenumber is large. In contrast, for $P > \kappa$ the distributions are non-trivial for moderate values of the evanescence parameter ζ . This means that for $P \leq \kappa$ one can safely choose only propagative plane waves, as we already know from Section 4.4, while for $P > \kappa$ evanescent waves are needed and their choice is non-trivial.

Parameter sampling. For any P we generate $M = \nu N(P)$ samples in the cylinder Y using the technique called *Inversion Transform Sampling* (ITS) [10, Sec. 5.2]. It consists in first generating sampling sets in the unit square $[0, 1]^2$ that converge (in a suitable sense) to the uniform distribution $\mathcal{U}_{[0,1]^2}$ when $M \rightarrow \infty$,

$$\{\mathbf{z}_m\}_m, \quad \text{with} \quad \mathbf{z}_m = (z_{m,\varphi}, z_{m,\zeta}) \in [0, 1]^2, \quad m = 1, \dots, M, \quad (8.2)$$

and then map back to the cylinder Y , to obtain sampling sets that converge to the probability density function $\rho_{N(P)}$ when $M \rightarrow \infty$, namely

$$\{\mathbf{y}_m\}_m, \quad \text{with} \quad \mathbf{y}_m := (2\pi z_{m,\varphi}, \Upsilon_N^{-1}(z_{m,\zeta})) \in Y, \quad m = 1, \dots, M. \quad (8.3)$$

In our case, the fact that the density function is constant with respect to φ considerably simplifies the generation of the samples and we don't need the techniques described in [10, Sec. 5] which rely on tensor-product like orthonormal basis (which we do not have). The inversion Υ_N^{-1} can be performed using elementary root-finding techniques. In our implementation we resort to the bisection method, which is both simple to use and robust. For practical implementations that need to perform this inversion step often, for instance in an adaptive setting, it is possible to reduce the cost of the inversion by performing an interpolation of the cumulative density function. The inversion procedure will then be simpler and cheaper.

In our numerical experiments we tested three types of sampling methods, which differ by how we generate the first sampling distribution $\{\mathbf{z}_m\}_m$ in the unit square:

1. *deterministic* sampling: the initial samples in the unit square are a tensor product of two sets of equispaced points with the same number of points in both directions (all numerical results presented are obtained by using as approximation set dimension the smallest square integer larger than or equal to M);
2. *Sobol* sampling: the initial samples in the unit square corresponds to Sobol sequences which are quasi-random low-discrepancy sequences²;

²We used the JULIA packages `Sobol.jl` and `QuasiMonteCarlo.jl`, which are themselves based on [5, 24]

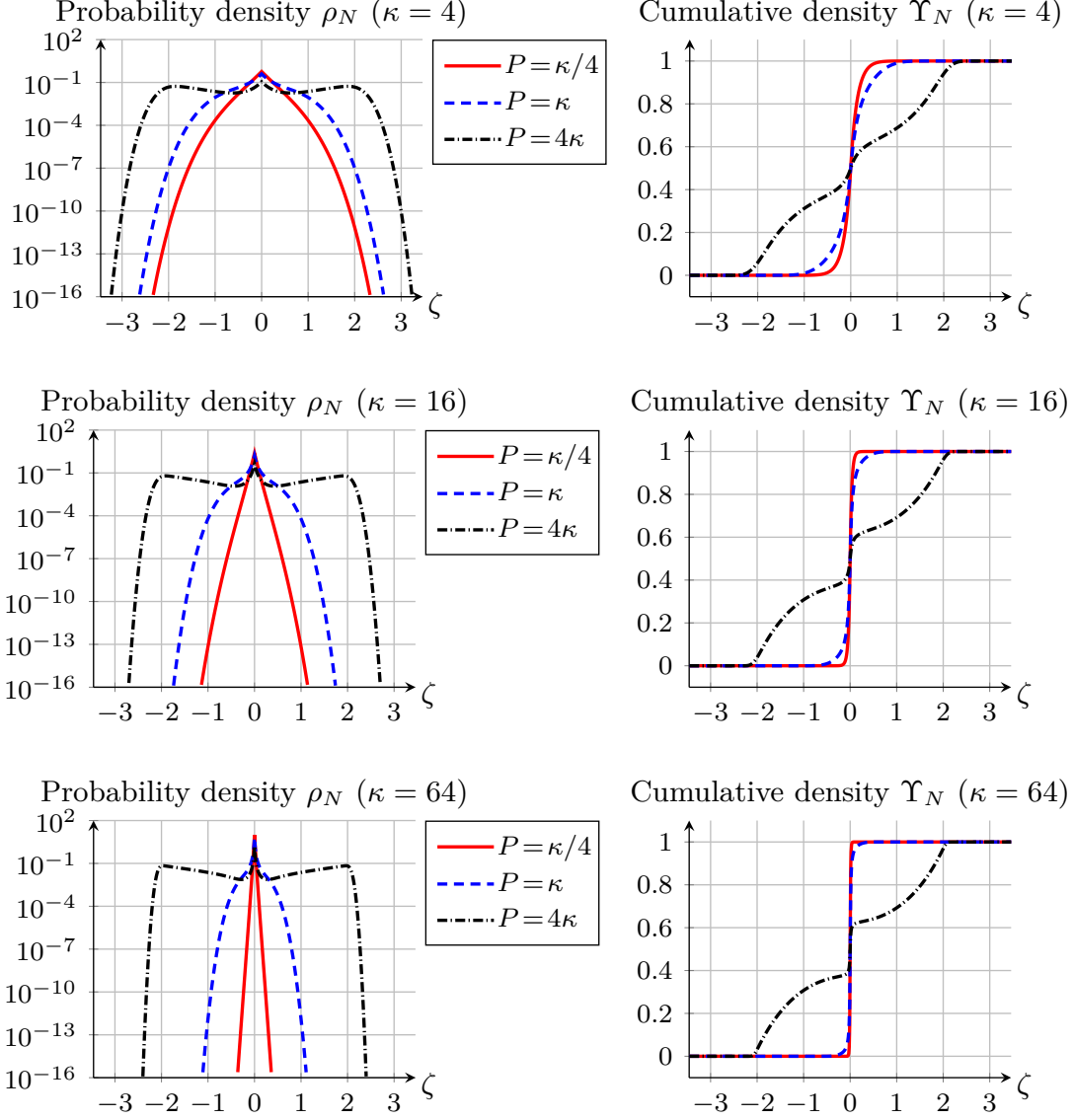


Figure 7: Sampling density functions $\rho_{N(P)}$ (left) and $\Upsilon_{N(P)}$ (right) with respect to the evanescence parameter ζ constructed for the subspace \mathcal{A}_P . The wavenumber κ varies in $\{4, 16, 64\}$ from top to bottom.

3. *random* sampling: the initial samples in the unit square are drawn randomly according to the product of two uniform distributions $\mathcal{U}_{[0,1]}$.

Some examples of sampling sets corresponding to the probability density function ρ_N for $\kappa = 16$ are reported in Figure 8. For these examples the number of sampling nodes is set to $M = \nu N(P)$ with $\nu = 4$, for the three types of sampling considered.

As expected, the sampling points cluster near the line $\zeta = 0$ for smaller P . This is the regime for which we know that propagative plane waves alone already provide a good approximation. However, there are no purely propagative plane waves $\zeta = 0$ as ρ_N is a continuous distribution. When $P > \kappa$ the evanescence parameter ζ spreads in a wider domain, with some clustering at the secondary modes of the distribution, in agreement with Figure 7.

8.2 Evanescent plane waves are stable

We return now to the numerical test which highlighted the instability of any approximation with *propagative* plane waves, see Section 4.3. We investigate whether our proposed method using *evanescent* plane waves exhibits better stability properties while not compromising the accuracy of the approximation.

The setting is the same, namely we compute approximation of the circular waves b_p for various p . The difference is that now we use the approximation sets $\Phi_{P,M}$ defined in (7.17), for which the M evanescent plane waves have parameters $\{\mathbf{y}_{P,M,m}\}_{m=1}^M$ computed as in (8.3), i.e. distributed according to the sampling distribution $\rho_{N(P)}$ defined in (7.9). These evanescent plane waves are normalized as in (7.17). Here the parameter P used to generate the M samples (that are adapted to the space \mathcal{A}_P) is set to 4κ .

The numerical results are reported in Figure 9. On the left panel we report the relative residual \mathcal{E} defined in (3.22) as a measure of the accuracy of the approximation. On the right panel we report the size of the coefficients, namely $\|\xi_{S,\epsilon}\|_{\ell^2}$, as a measure of the stability of the approximation. These figures should be compared to Figure 3, which are the corresponding results when only purely propagative plane waves are used in the approximation set (see (4.3)).

The main observation is that by using sufficiently many waves (i.e. setting M sufficiently large, of the order of $M = 32\kappa \approx 4N(P)$) we are now able to approximate to (almost) machine precision all the modes $|p| \leq P = 4\kappa$. This includes the propagative modes $|p| \leq \kappa$ (which were already well-approximated by purely propagative plane waves), but more importantly, this also includes evanescent modes $\kappa < |p| \leq P = 4\kappa$, for which purely propagative plane waves failed to provide any meaningful approximation. Moreover, even much higher modes $|p| > P = 4\kappa$ are approximated to acceptable accuracy.

Further, we stress that the norms of the coefficients $\|\xi_{S,\epsilon}\|_{\ell^2}$ used in the approximate expansions remain moderate. This is in stark contrast with the results of Section 4.3, where the exponential growth of the coefficients prevented any accurate numerical approximation.

Comparing Figures 10 and 4, the condition number (ratio of the largest singular value σ_{\max} over the smallest σ_{\min}) of the matrix A is of the same order for propagative and evanescent plane waves, when M is large enough. The improved accuracy (for evanescent modes) is not due to an improved conditioning of the underlying linear system but to an increase of the ϵ -rank (i.e. the number of singular values larger than ϵ) of the matrix (from less than 100 for propagative plane waves to around 250 for evanescent plane waves in the case $M = 32\kappa$). To further increase the ϵ -rank, one needs to increase the truncation parameter P .

Comparing Figure 9 and Figure 3, we see that for small M (e.g. $M = 4\kappa$ and $M = 8\kappa$) purely propagative plane waves provide better approximation of propagative modes than evanescent plane waves. This is because the approximation spaces made of propagative plane waves are

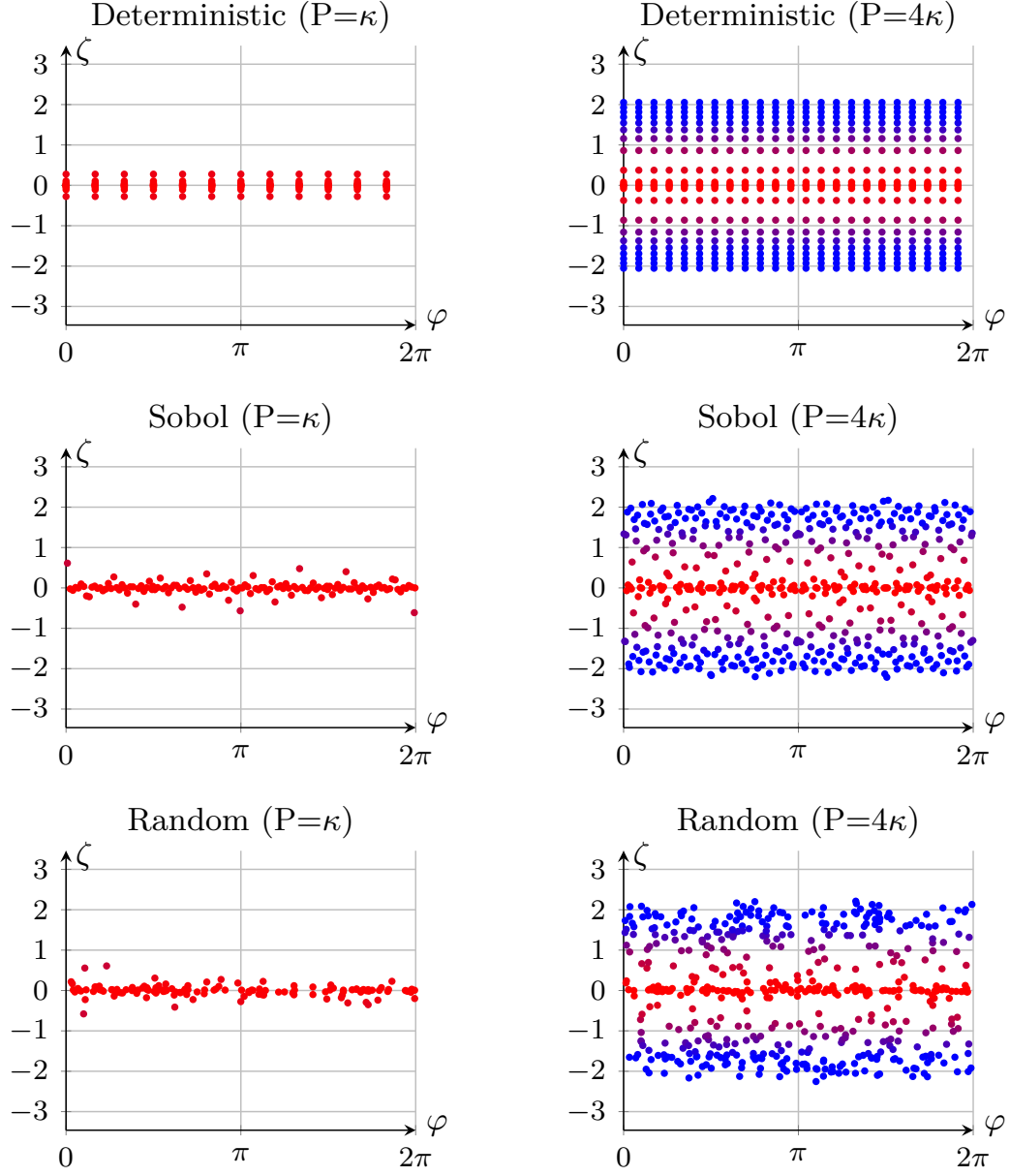
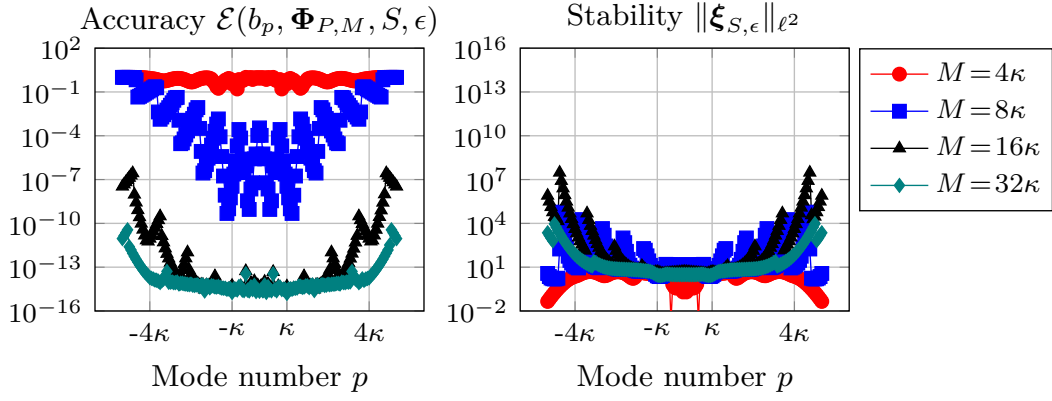
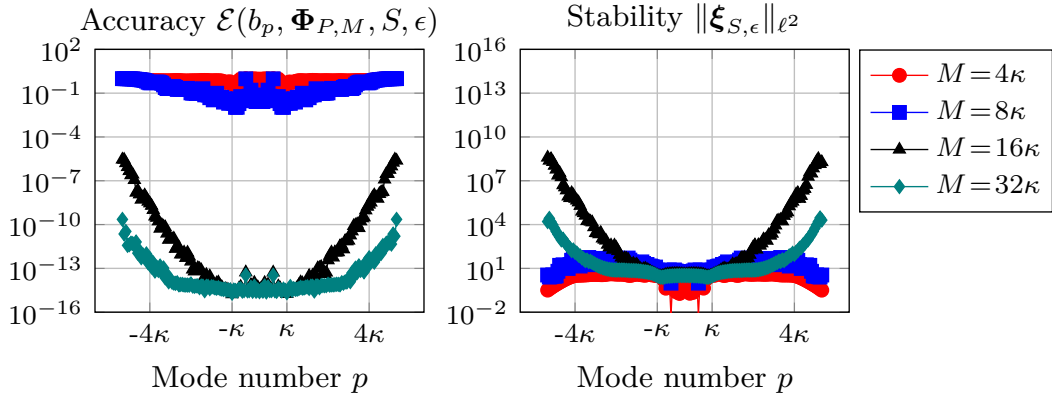


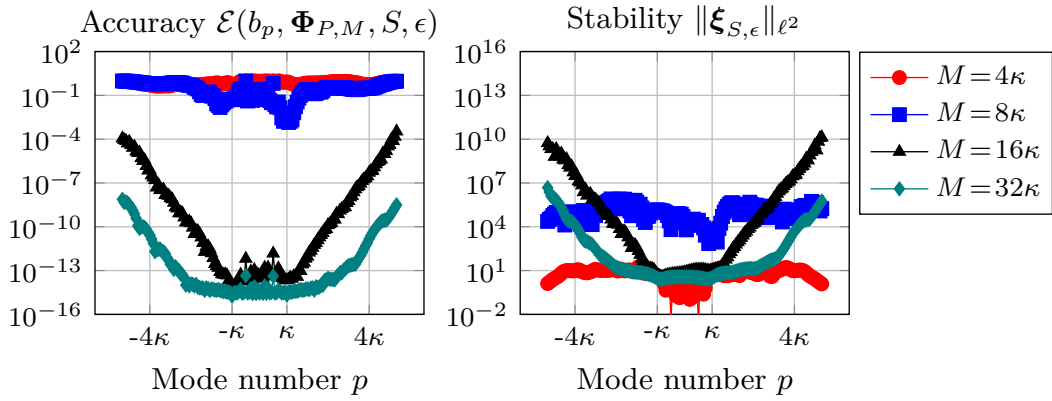
Figure 8: $M = 4N(P)$ samples in the cylinder Y for P equal to κ (left) and 4κ (right) and for various types of sampling method (from top to bottom). Wavenumber $\kappa = 16$.



(a) Deterministic sampling



(b) Sobol sampling



(c) Random sampling

Figure 9: Accuracy \mathcal{E} , as defined in (3.22), (left) and stability $\|\xi_{S,\epsilon}\|_{\ell^2}$ (right) of the approximation of circular waves b_p by evanescent plane waves. Truncation at $P = 4\kappa$, wavenumber $\kappa = 16$.

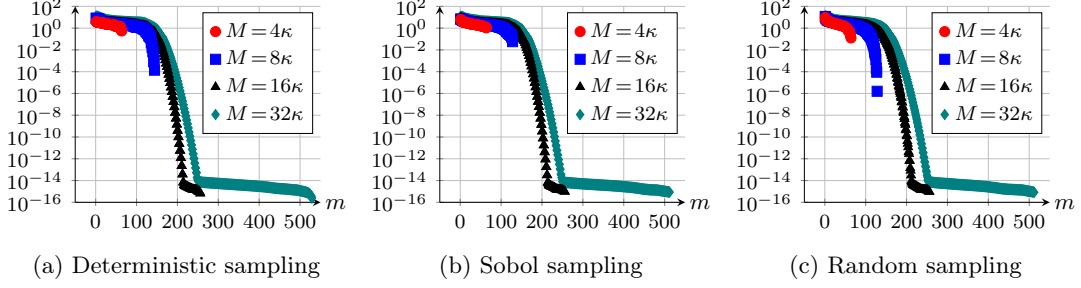


Figure 10: Singular values $\{\sigma_m\}_{m=1}^M$ of the matrix A when using a set of M evanescent plane waves. Truncation at $P = 4\kappa$, wavenumber $\kappa = 16$.

tuned for propagative modes, which span a space of dimension $2\kappa + 1$. In contrast, the approximation spaces made of evanescent plane waves target a larger number of modes, including some evanescent modes, which span a space of dimension $N = 2P + 1$ with $P = 4\kappa$ in this numerical experiment. For a general target solution containing evanescent modes, one does not expect any advantage in using propagative plane waves only.

8.3 Approximation of solution surrogates

We test the procedure described so far by reconstructing some solution surrogates of the form

$$u := \sum_{|p| \leq P} \hat{u}_p b_p \in \mathcal{B}_P. \quad (8.4)$$

The coefficients $\{\hat{u}_p\}_{|p| \leq P}$ of the Fourier–Bessel expansion that make up u are products of normally-distributed random numbers (with mean 0 and standard deviation 1) and the scaling factors $[\max(1, |p| - \kappa)]^{-1/2}$. The coefficients of any element of \mathcal{B} decay in modulus as $o(|p|^{-1/2})$ for $|p| \rightarrow \infty$; this is therefore a rather difficult scenario for an approximation problem.

We then apply the procedure described above for the three types of sampling strategies considered. The sampling points are constructed knowing that $T^{-1}u$ is an element of \mathcal{A}_P . In other words, the optimal modal truncation parameter $P^* = P$ (where P appears in (8.4)) is assumed to be known in this numerical experiment. The main purpose is to investigate the validity of Conjecture 7.1. We study here the convergence of the error with respect to the dimension of the approximation space M . The number of sampling points on the boundary of the disk is set to $S = 2M$.

The numerical results are given in Figure 11. On the left panel we report the relative residual \mathcal{E} , defined in (3.22), as a measure of the accuracy of the approximation. On the right panel we report the size of the coefficients, namely $\|\xi_{S,\epsilon}\|_{\ell^2}/\|u\|_{\mathcal{B}}$, as a measure of the stability of the approximation.

The main observation is that the error quickly decays with respect to the ratio $M/N(P) = M/(2P + 1)$, which represents the ratio of the dimension of the approximation set over the dimension of the space the solution surrogate lives in. When P is large enough (say $P \geq 2\kappa$ which remains moderate), the decay is relatively independent of P .

The second observation is that the norm of the coefficients $\|\xi_{S,\epsilon}\|_{\ell^2}/\|u\|_{\mathcal{B}}$ in the expansions is a decreasing function of the size M of the approximation space. We see once more that one gets accurate and stable approximations. The values of $\|\xi_{S,\epsilon}\|_{\ell^2}/\|u\|_{\mathcal{B}}$ reported for small values

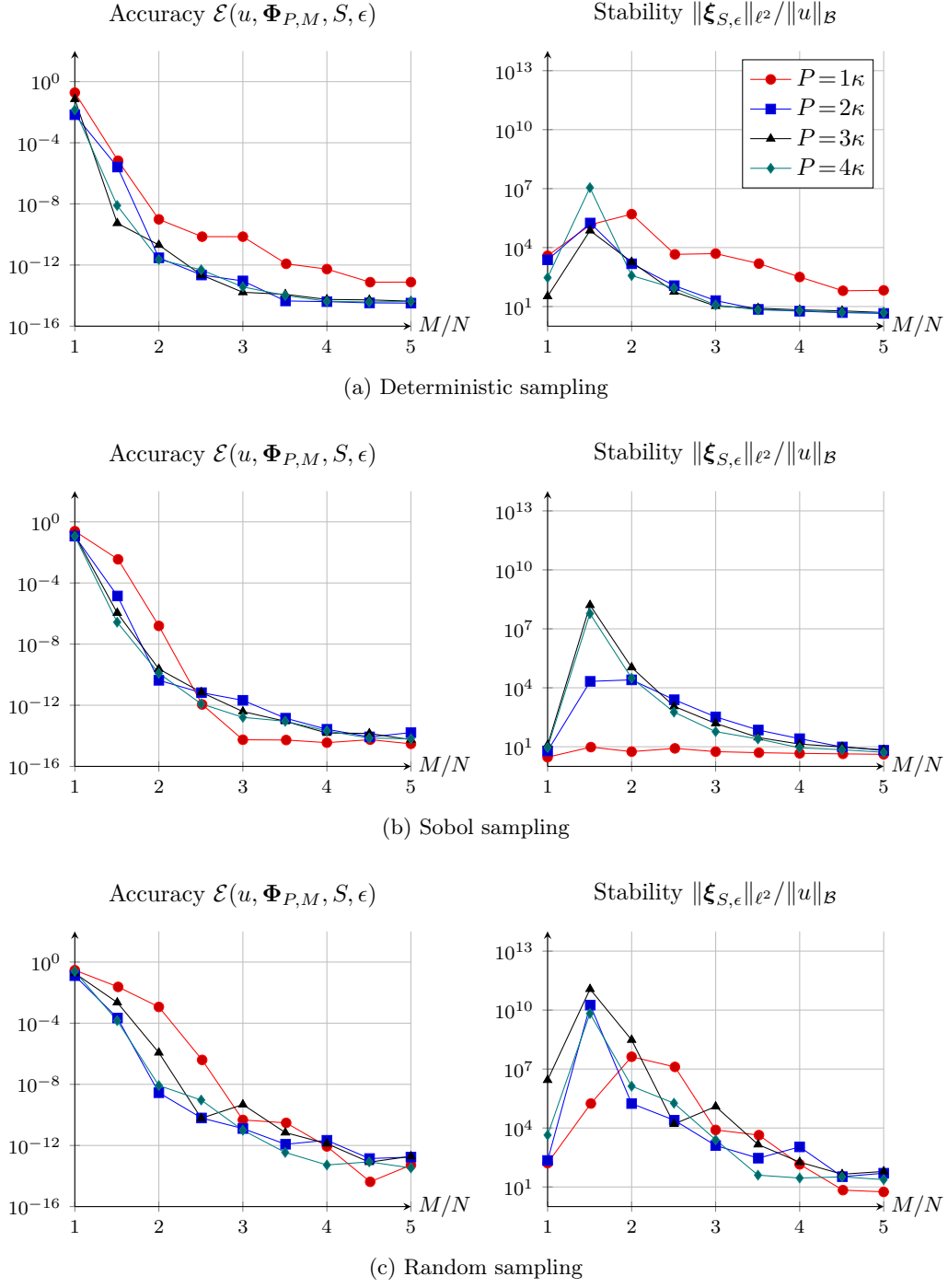


Figure 11: Accuracy \mathcal{E} , as defined in (3.22), (left) and stability $\|\xi_{S,\epsilon}\|_{\ell^2}/\|u\|_{\mathcal{B}}$ (right) of the approximation by M evanescent plane waves of solution surrogates u in the form (8.4) that belong to the space \mathcal{B}_P of dimension $N(P) = 2P + 1$. The horizontal axis represents the ratio $M/N(P)$. Wavenumber $\kappa = 16$.

of $M/N(P)$ (in particular the increase at the start) are not significant since they correspond to inaccurate approximations.

We report in Figure 12 the plots of a solution surrogate (8.4) for a larger frequency $\kappa = 64$ and truncation parameter $P = 3\kappa = 192$. The approximation error when using $M = 3(2P+1) = 1155$ plane waves, either propagative or evanescent (with points in Y sampled as a Sobol sequence) is also given. In the first case the absolute error in the disk is much larger (more than 12 orders of magnitude larger if measured in $L^\infty(B_1)$ norm) and concentrated near the boundary. The number of degrees of freedom per wavelength $\lambda = 2\pi/\kappa$ used in each direction can be estimated by $\lambda\sqrt{M}/\pi \approx 1.9$ (here π represents the area of the unit disk). For low order methods, a commonly used rule of thumb is to use around $6 \sim 10$ degrees of freedom per wavelength to have 1 or 2 digits of accuracy. We see that we get 12 digits of accuracy for only a fraction of this number. For $M = 2(2P+1) = 770$, the maximum absolute error reached is measured to $1.3 \cdot 10^{-10}$ (not plotted).

Overall, the numerical results validate Conjecture 7.1.

8.4 Numerical evidence of quasi-optimality

An important question regarding the efficiency of the proposed method concerns how the size of the approximation set M should vary with respect to the truncation parameter P . Fixing P amounts to look at the finite dimensional subspace \mathcal{B}_P which contains the first $N(P) = 2P+1$ modes. Since N is the dimension of \mathcal{B}_P there is no hope to have approximation spaces with dimension $M < N$ that are able to approximate all elements of this space. An *optimal* approximation set would therefore achieve this with $M = N$ elements at best. We show below numerical evidence that we achieve *quasi-optimality* in the sense that our approximation spaces $\Phi_{P,M}$ defined in (7.17) only need $M = \mathcal{O}(N)$ with a moderate proportionality constant to approximate the N circular modes with reasonable accuracy.

We investigate numerically the linearity of the relation $P \rightarrow M^*(u, P, \eta)$, as defined in (7.16) (for fixed u and η), namely the validity of a law of the form $M^*(u, P, \eta) \approx \nu N(P) = \nu(2P+1)$ for some $\nu = \nu(u, \eta) > 0$. To do this, for some $\sigma > 0$, we vary P and compute

$$\widetilde{M}^* = \widetilde{M}^*(P, \sigma) := \min \{M \in \mathbb{N} \mid \mathcal{E}(b_p, \Phi_{P,M}, S, \epsilon) \leq \sigma, \forall |p| \leq P\}, \quad (8.5)$$

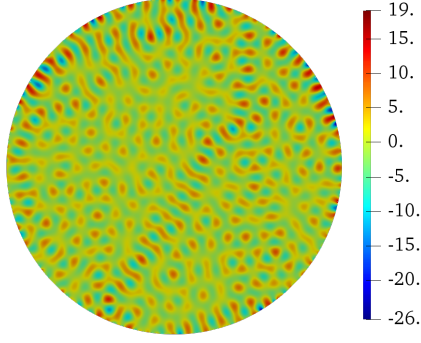
where \mathcal{E} was defined in (3.22). The quantity \widetilde{M}^* is expected to be a good estimate of

$$\max_{|p| \leq P} M^*(b_p, P, \eta), \quad (8.6)$$

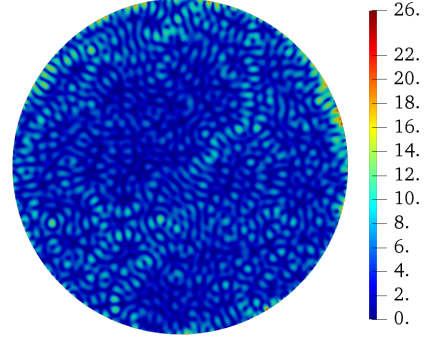
where $M^*(u, P, \eta)$ was defined in (7.16). The number of sampling points on the boundary of the disk is set to $S = 2M$.

The numerical results are given in Figure 13 for the accuracy level $\sigma = 10^{-12}$. We represent here the variation of the ratio $\widetilde{M}^*(P, \sigma)/N(P)$ with respect to the truncation parameter P . If the optimal law for $\widetilde{M}^*(P, \epsilon)$ was linear with respect to P , we would expect constant values. Regardless of the type of sampling that is performed, we observe decreasing curves that converge to some optimal asymptotic value for ν . The asymptotic value reached, falls within the range $[3, 6]$ which is rather moderate, and varies with the type of sampling considered. This means that the first N circular modes (propagative and evanescent) can be stably approximated with uniform relative error $\leq 10^{-12}$ using roughly $3N$ to $6N$ plane waves. Moreover, this asymptotic behavior seems to be robust with respect to the wavenumber κ .

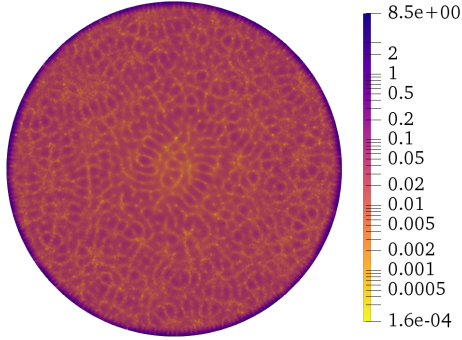
These more systematic results confirm what was already observed in Section 8.3. The behavior of the optimal asymptotic \widetilde{M}^* with respect to $N(P)$ seems indeed to be linear or even sub-linear.



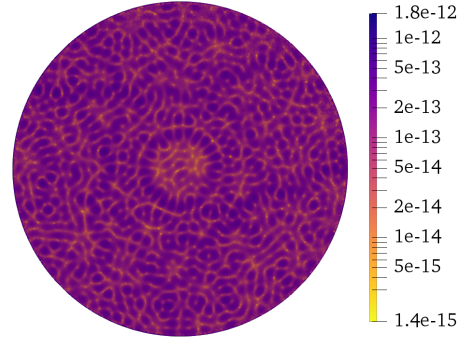
(a) Real part of target solution $\Re u$



(b) Modulus of target solution $|u|$



(c) Absolute error using PPW $|u - \mathcal{T}_{\Phi_M} \xi_{S,\epsilon}|$



(d) Absolute error using EPW $|u - \mathcal{T}_{\Phi_{P,M}} \xi_{S,\epsilon}|$

Figure 12: Solution surrogate u , target of the approximation, defined in (8.4) with $P = 3\kappa = 192$ (top) and associated absolute errors when approximated by $M = 3(2P + 1) = 1155$ plane waves, either propagative ones Φ_M from (4.3) (bottom left) or evanescent ones $\Phi_{P,M}$ from (7.17) whose parameters are constructed using a Sobol type sampling (bottom right). Note the different color scales. The colormaps associated to absolute errors are logarithmic for better visualization. Wavenumber $\kappa = 64$.

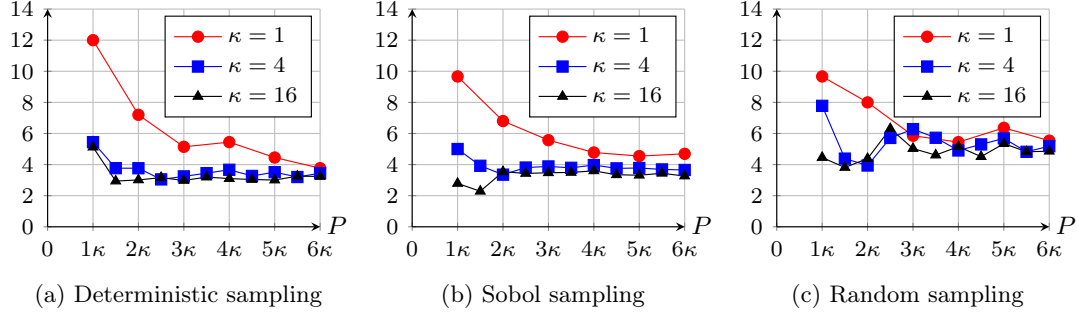


Figure 13: Ratio $\widetilde{M}^*(P, \sigma)/N(P)$ with respect to the truncation parameter P for various types of sampling method and $\sigma = 10^{-12}$.

9 Conclusions

Ill-conditioning, which is inherent in the Trefftz schemes we are interested in, can be overcome if there exist accurate approximations that are moreover stable (i.e. expansions with bounded coefficients). To approximate Helmholtz solutions, propagative plane waves are known to provide accurate approximations. However, the associated expansions are necessarily *unstable*: the norm of the coefficients blow up for solutions with high-frequency content. In contrast, evanescent plane waves, which contain high-frequency evanescent plane waves, give accurate as well as *stable* results. To construct stable sets of evanescent plane waves, we show numerically that an effective strategy is to sample the parametric domain according to the measure ρ_N .

This paper is only the first step towards stable and accurate approximation schemes based on evanescent plane waves. Next steps include the extensions to more general geometries, three-dimensional problems, time-harmonic Maxwell and elastic wave equations, the application to Trefftz schemes and to sound-field reconstruction algorithms. A theoretical problem that we have left open is the proof of Conjecture 7.1, under appropriate assumptions on the convergence of the sampling nodes.

Acknowledgements The authors are grateful to Ralf Hiptmair for helpful discussions. AM and EP acknowledge support from PRIN project “NA-FROM-PDEs” and from MIUR through the “Dipartimenti di Eccellenza” Program (2018–2022) — Dept. of Mathematics, University of Pavia.

References

- [1] B. Adcock and D. Huybrechs. “Frames and numerical approximation”. In: *SIAM Rev.* 61.3 (2019), pp. 443–473.
- [2] B. Adcock and D. Huybrechs. “Frames and numerical approximation II: Generalized sampling”. In: *J. Fourier Anal. Appl.* 26.6 (2020), Paper No. 87, 34.
- [3] P. R. Antunes. “A numerical algorithm to reduce ill-conditioning in meshless methods for the Helmholtz equation.” In: *Numer. Algorithms* 79.3 (2018), pp. 879–897.
- [4] H. Barucq, A. Bendali, J. Diaz, and S. Tordeux. “Local strategies for improving the conditioning of the plane-wave ultra-weak variational formulation”. In: *J. Comput. Phys.* 441 (2021), Paper No. 110449, 18.

- [5] P. Bratley and B. L. Fox. “Algorithm 659: Implementing Sobol’s quasirandom sequence generator”. In: *ACM Trans. Math. Software* 14.1 (1988), pp. 88–100.
- [6] O. Cessenat and B. Despres. “Application of an ultra weak variational formulation of elliptic PDEs to the two-dimensional Helmholtz problem”. In: *SIAM J. Numer. Anal.* 35.1 (1998), pp. 255–299.
- [7] S. Chaillat and F. Collino. “A wideband fast multipole method for the Helmholtz kernel: theoretical developments”. In: *Comput. Math. Appl.* 70.4 (2015), pp. 660–678.
- [8] G. Chardon, A. Cohen, and L. Daudet. “Sampling and reconstruction of solutions to the Helmholtz equation”. In: *Sampl. Theory Signal Image Process.* 13.1 (2014), pp. 67–89.
- [9] O. Christensen. *An introduction to frames and Riesz bases*. Second. Applied and Numerical Harmonic Analysis. Birkhäuser/Springer, [Cham], 2016, pp. xxv+704.
- [10] A. Cohen and G. Migliorati. “Optimal weighted least-squares methods”. In: *SMAI J. Comput. Math.* 3 (2017), pp. 181–203.
- [11] D. Colton and P. Monk. “A novel method for solving the inverse scattering problem for time-harmonic acoustic waves in the resonance region”. In: *SIAM J. Appl. Math.* 45.6 (1985), pp. 1039–1053.
- [12] S. Congreve, J. Gedicke, and I. Perugia. “Numerical investigation of the conditioning for plane wave discontinuous Galerkin methods”. In: *European Conference on Numerical Mathematics and Advanced Applications*. Springer. 2017, pp. 493–500.
- [13] D. Colton and R. Kress. *Inverse acoustic and electromagnetic scattering theory*. 3rd ed. English. Vol. 93. New York, Springer, 2013, pp. xiv + 405.
- [14] E. Deckers, O. Atak, L. Coox, R. D’Amico, H. Devriendt, et al. “The wave based method: an overview of 15 years of research”. In: *Wave Motion* 51.4 (2014), pp. 550–565.
- [15] *NIST Digital Library of Mathematical Functions*. <http://dlmf.nist.gov/>, Release 1.1.1 of 2021-03-15. F. W. J. Olver, A. B. Olde Daalhuis, D. W. Lozier, B. I. Schneider, R. F. Boisvert, C. W. Clark, B. R. Miller, B. V. Saunders, H. S. Cohl, and M. A. McClain, eds.
- [16] D. Freeman and D. Speegle. “The discretization problem for continuous frames”. In: *Adv. Math.* 345 (2019), pp. 784–813.
- [17] K. Gröchenig. “Sampling, Marcinkiewicz-Zygmund inequalities, approximation, and quadrature rules”. In: *J. Approx. Theory* 257 (2020), pp. 105455, 20.
- [18] M. Hahmann, S. A. Verburg, and E. Fernandez-Grande. “Spatial reconstruction of sound fields using local and data-driven functions”. In: *J. Acoust. Soc. Am.* 150.6 (2021), pp. 4417–4428.
- [19] J. Hampton and A. Doostan. “Coherence motivated sampling and convergence analysis of least squares polynomial Chaos regression”. In: *Comput. Methods Appl. Mech. Engrg.* 290 (2015), pp. 73–97.
- [20] R. Hiptmair, A. Moiola, and I. Perugia. “A survey of Trefftz methods for the Helmholtz equation”. In: *Building bridges: connections and challenges in modern approaches to numerical partial differential equations*. Vol. 114. Lect. Notes Comput. Sci. Eng. Springer, [Cham], 2016, pp. 237–278.
- [21] T. Huttunen, P. Gamallo, and R. J. Astley. “Comparison of two wave element methods for the Helmholtz problem”. In: *Comm. Numer. Methods Engrg.* 25.1 (2009), pp. 35–52.
- [22] D. Huybrechs and A.-E. Olteanu. “An oversampled collocation approach of the wave based method for Helmholtz problems”. In: *Wave Motion* 87 (2019), pp. 92–105.

- [23] W. Jin and W. B. Kleijn. “Theory and design of multizone soundfield reproduction using sparse methods”. In: *IEEE Trans. Audio Speech Lang. Process* 23.12 (2015), pp. 2343–2355.
- [24] S. Joe and F. Y. Kuo. “Remark on Algorithm 659: implementing Sobol’s quasirandom sequence generator”. In: *ACM Trans. Math. Software* 29.1 (2003), pp. 49–57.
- [25] T. Luostari, T. Huttunen, and P. Monk. “Improvements for the ultra weak variational formulation”. In: *Internat. J. Numer. Methods Engrg.* 94.6 (2013), pp. 598–624.
- [26] J. M. Melenk. “On generalized finite element methods”. PhD thesis. Univ. of Maryland, 1995.
- [27] A. Moiola, R. Hiptmair, and I. Perugia. “Plane wave approximation of homogeneous Helmholtz solutions”. In: *Z. Angew. Math. Phys.* 62.5 (2011), pp. 809–837.
- [28] V. I. Paulsen and M. Raghupathi. *An introduction to the theory of reproducing kernel Hilbert spaces*. Vol. 152. Cambridge Studies in Advanced Mathematics. Cambridge University Press, Cambridge, 2016, pp. x+182.
- [29] E. Perrey-Debain. “Plane wave decomposition in the unit disc: convergence estimates and computational aspects”. In: *J. Comput. Appl. Math.* 193.1 (2006), pp. 140–156.
- [30] S. A. Verburg and E. Fernandez-Grande. “Reconstruction of the sound field in a room using compressive sensing”. In: *J. Acoust. Soc. Am.* 143.6 (2018), pp. 3770–3779.
- [31] N. Weck. “Approximation by Herglotz wave functions”. In: *Math. Methods Appl. Sci.* 27.2 (2004), pp. 155–162.